SOLUTE TRANSPORT IN HETEROGENEOUS POROUS MEDIA

by

Xiaomin Zhao and M. Nafi Toksöz

Earth Resources Laboratory
Department of Earth, Atmospheric, and Planetary Sciences
Massachusetts Institute of Technology
Cambridge, MA 02139

ABSTRACT

Solute mass transport in porous media is strongly correlated with pore fluid flow. The analysis of solute transport is an effective means for studying medium heterogeneities. In this study, we discuss the effects of heterogeneity on the tracer transport. Assuming steady fluid flow, we have simulated tracer transport in various permeability heterogeneities. The results show that the tracer distribution is very closely correlated with the medium heterogeneity, and anisotropy in tracer transport exists when there is permeability lineation and large permeability contrast between low- and high-permeability regions. An important feature by which the tracer transport differs from the fluid flow field is that the tracer transport tends to smear the effects of a thin non-permeable layer (or small permeability barriers) through diffusion into the low-permeability layer, while the fluid flow cannot penetrate the low-permeability layer. In addition, the modeling results also show that the tracer transport strongly depends on the tracer source dimension, as well as the flow source dimension.

INTRODUCTION

The problem of solute transport associated with fluid flow in porous media has become increasingly important in geophysical applications. In petroleum reservoir production, tracer transport tests are a common technique to study the interwell connectivity of a reservoir and anisotropy of reservoir permeability. These tests are also very useful in studying connectivity of a borehole fracture network (Raven and Novakowski, 1984). In environmental studies, the knowledge of contaminant transport and its spatial distributions is essential for designing field survey and remediations. The heterogeneity variations in a porous medium can have significant effects on the transport process. Numerous works have been performed to study the relationship between heterogeneity and the transport process. Atal *et al.* (1988) have studied how the macroscopic and microscopic fluid dispersion varies with reservoir heterogeneities. Tsang *et al.* (1988) and Moreno *et al.* (1988) used the existing flow field to predict the movement of solute concentration through a rough surface fracture using partical tracking techniques. Thompson (1991) has investigated the fluid transport problem in natural fractures with rough surfaces. Thompson (1991) showed that the surface roughness creates spatially

varying hydraulic conductivity along the fracture; it therefore causes fluid flow and tracer transport to be restricted to channels that occupy only a small percentage of the fracture volumes, resulting in significant channeling of the transport. Because of the heterogeneous nature of a geological medium, the solute transport in heterogeneous porous media can provide knowledge about the effects of heterogeneities on the solute transport and transport parameters that control these effects. As a result, such effects as permeability heterogeneity, permeability anisotropy, *etc.*, can be estimated from measuring the solute mass transport behaviors in a reservoir. The primary goal of this study is to investigate the effects of formation permeability heterogeneity and anisotropy on the solute transport characteristics measured downhole.

The governing equation for the solute mass transport problem is the advection-dispersion equation. For heterogeneous media, numerical models can easily deal with variability in the flow and transport parameters (for example, permeability, porosity, and dispersivity *etc.*). Thus they can be conveniently used to model geological structures with complex geometry. This study adopts an Alternating Direction Implicit (ADI, Ferziger, 1980; Zhao and Toksöz, 1992) finite difference scheme to solve the time-dependent tracer transport problem. By substituting the domain of fluid flow into the finite difference grid, varying parameter values are assigned to the numerical grid to account for medium heterogeneities, and the ADI finite difference technique is used to calculate the solute distribution at each given time step. In this way, we can simulate the complex solute plume shapes that develop in natural geological systems.

Complicating the solute transport problem is the fluid velocity field that is very important in determining the advection of the transport process. Continuity conditions in the numerical solutions of the transport equation require an accurate representation of the velocity field. The fluid flow velocity field is obtained from simulation of flow in the heterogeneous porous medium, in which the velocity field is calculated using Darcy's law with given permeability distribution and known parameters and boundary conditions. This problem has been solved in Zhao and Toksöz, (1991). The fluid flow field is assumed to be independent of the solute transport. In other words, the solute concentration does not influence the flow. In this situation, the flow and transport equations can be solved separately.

THE ADVECTION-DIFFUSION-DISPERSION EQUATION FOR SOLUTE TRANSPORT

For fluid flow in a porous medium, solute transports are due to three important mechanisms: diffusion, dispersion, and advection. Here we briefly describe the derivation of the advection-diffusion-dispersion equation, in order to introduce the flow and transport parameters that control the transport process. The solute mass transport equation is based on the mass conservation equation:

$$\nabla \cdot \vec{J} = -\frac{\partial}{\partial t}(\phi C) \tag{1}$$

where $\vec{J}$ is the solute mass flux, ϕ is porosity, and C is solute concentration. The product ϕC is mass per volume. Equation (1) states that the net mass output per unit volume

equals the time rate of change of mass within the volume.

The flux $\vec{J}$ contains both diffusion flux and advection flux:

$$\vec{J} = -\phi D_0 \nabla C + \vec{v}(\phi C). \tag{2}$$

The first term on the right hand side is the diffusion flux, D_0 being the molecular diffusion coefficient. The second term is the advection flux, which is caused by $\vec{v}$, the velocity of the pore fluid flow.

During mass transport, mechanical dispersion is also an important mechanism (Tang *et al.*, 1981; Sudicky and Frind, 1982; Grisak and Pickens, 1980). The effect of this dispersion is mathematically treated by changing the D_0 in Equation (2) to (Domenico and Schwartz, 1990; Thompson, 1991)

$$D = D_0 + \alpha U \tag{3}$$

where α is known as the dynamic dispersivity which is an important property of the porous medium. The coefficient D now is called the hydrodynamic dispersion coefficient. Depending on the value of α, the dispersive process due to the fluid velocity U contributes to the mechanical mixing of solute. Here U is the magnitude of the velocity. In the case of multi-dimensional flow, U is defined as

$$U = ||\vec{v}|| = \sqrt{v_x^2 + v_y^2 + v_z^2}. \tag{4}$$

This approach was used by Murty and Scott (1977), who assumed that D is proportional to the full magnitude of fluid flow velocity. For a heterogeneous porous medium, we also allow $\bar{v}$ to vary spatially if the velocity field varies because of permeability variation of the medium. In this case, $U = U(x, y, z)$ is the local magnitude of the velocity field. Letting U vary spatially is important for modeling solute transport in a heterogeneous porous medium, because in such a medium velocity values may differ greatly at different locations of the medium, especially if the driving pressure is a localized (or point) source. By substituting Equations (2) and (3) into Equation (1), we get

$$\nabla \cdot [\phi D \nabla C] - \nabla \cdot [\vec{v}(\phi C)] = \frac{\partial(\phi C)}{\partial t} \quad . \tag{5}$$

The second term on the left hand side of Equation (5) can be written as

$$\nabla \cdot [\vec{v}(\phi C)] = (\nabla \cdot \vec{v})\phi C + \vec{v} \cdot \nabla(\phi C) \quad . \tag{6}$$

If we assume that the solute transport process does not change the density of the fluid, then the solute transport does not affect the flow velocity field $\vec{v}$, and $\vec{v}$ can be calculated independent of the solute concentration field. We further assume that solute transport takes place in a steady fluid flow field, which is governed by Darcy's law $\vec{v} = -\kappa/\mu \nabla P$, where κ is permeability, μ is fluid viscosity and ∇P is the pressure gradient. In this case, the divergence of the fluid velocity field vanishes, as in the following equation,

$$\nabla \cdot \vec{v} = \nabla \cdot \left(\frac{\kappa}{\mu} \nabla P\right) = 0. \tag{7}$$

Equation (5) is the governing equation for the fluid pressure in a porous medium with a heterogeneous permeability distribution, which can be solved to compute the fluid velocity field $\vec{v}$ for the given permeability distribution and boundary conditions (see Zhao and Toksöz, 1991). Under the steady state flow assumption, Equation (5) is simplified to become

$$\nabla \cdot [\phi D \nabla C] - \vec{v} \cdot \nabla(\phi C) = \frac{\partial(\phi C)}{\partial t} \quad . \tag{8}$$

Equation (8) is the governing equation for solute transport in a steady fluid flow field. This equation includes the effects of diffusion, dispersion, and advection transport in heterogeneous media. This equation is the basis for the numerical modeling of solute transport in heterogeneous media. From the governing equation, it can be seen that the solute transport is a complicated process affected by a number of factors. Because of the molecular diffusion process, over a certain period of time diffusion can cause solute mass to move considerable distances, even in media with very low permeability. The pore fluid velocity field $\vec{v}$ plays an important role in the solute transport process. Therefore diffusion and advection processes compete with each other in the transport process. When diffusion dominates, the solute tends to be homogeneously dispersed in the medium. On the other hand, according to Darcy's law, the velocity field $\vec{v}$ is controlled by medium permeability and the pressure gradient that drives the flow. Therefore, when advection dominates, the transport process will mainly reflect the effect of medium permeability. In this later case, effects of permeability and porosity heterogeneities become an important issue. Because of this mechanism, tracer tests are used as diagnostics of formation permeability.

The primary goal of this study is to investigate the effects of medium heterogeneous properties, especially permeability and porosity, on the solute transport process. Aimed at geophysical applications, we will model solute transport or tracer experiments made in boreholes, because the majority of such measurements are made downhole. The transport process will be simulated in a Cartesian coordinate system to study the vertical variation of solute concentration in the crosshole experiment. By modeling the transport process for a point source, we can also simulate the azimuthal variation of solute transport due to tracer injection from a borehole.

FORMULATION IN CARTESIAN COORDINATES

Theoretical formulation

In this study, we model solute transport in a two-dimensional domain. For the 2-D case, Equation (8) can be written as

$$\frac{\partial}{\partial x}\left(\phi D \frac{\partial C}{\partial x}\right) + \frac{\partial}{\partial z}\left(\phi D \frac{\partial C}{\partial z}\right) - v_x \frac{\partial(\phi C)}{\partial x} - v_z \frac{\partial(\phi C)}{\partial z} = \frac{\partial(\phi C)}{\partial t} \quad . \tag{9}$$

The pore fluid volumetric flow velocities v_x and v_z are computed as follows. We first solve the following equation for the pressure field

$$\frac{\partial}{\partial x}\left[\alpha(x,z)\frac{\partial P}{\partial x}\right] + \frac{\partial}{\partial z}\left[\alpha(x,z)\frac{\partial P}{\partial z}\right] = 0 \quad , \tag{10}$$

where $\alpha(x,z) = \dfrac{\kappa(x,z)K_f}{\mu\phi}$. Once the pressure field is found, the velocity field can be computed using Darcy's law, as given by

$$v_x = -\frac{\kappa(x,z)}{\mu}\frac{\partial P}{\partial x} \tag{11}$$

$$v_z = -\frac{\kappa(x,z)}{\mu}\frac{\partial P}{\partial z}. \tag{12}$$

Given the heterogeneous permeability distribution $\kappa(x,z)$ over the $x-$ and $z-$ system, Equation (10) is solved to yield the fluid flow velocity field $\vec{v}$ (v_x, v_z) (see Zhao and Toksöz, 1991). By substituting the known flow field into Equation (9), solute mass transport can be simulated for any given time by solving Equation (9). We use the finite difference method to solve Equations (9) and (10). In the finite difference scheme, a rectangular domain of dimensions $L_x \times L_z$ is discretized into a 2-D grid system. The solution procedure for Equation (10) has been described in Zhao and Toksöz, (1991).

To use the ADI finite difference scheme to solve Equation (9), we re-write the Equation (8) as follows (suppose the porosity ϕ does not change with time):

$$\nabla \cdot [\phi D \nabla C] - \phi\vec{v} \cdot \nabla C - \vec{v} \cdot \nabla\phi C = \phi\frac{\partial C}{\partial t} \quad . \tag{13}$$

For modeling effects of medium heterogeneities, porosity ϕ and permeability κ are represented using several random models. These models are isotropic random models and lineated random distributions generated using a Gaussian correlation function, a random flow channel model based on the lineated random distribution, and a flow channel model using the Poisson process. The generation of these random models is described in detail in Zhao and Toksz, (1991).

As a reasonable approximation, we assume that the porosity heterogeneity is correlated with permeability heterogeneity, because a high permeability rock generally has high porosity. Therefore, the same heterogeneity model can be used. This model is scaled by respective maximum permeability and porosity values to give the heterogeneous permeability and porosity distributions. In this way, high permeability regions correspond to high porosity regions while low permeability regions correspond to low porosity regions, allowing for the effective modeling of the effects of flow channels (high κ and ϕ) and flow barriers (low κ and ϕ).

Boundary Conditions

Boundary conditions are required to solve Equations (9) and (10). We will use four types of boundary conditions for the solute transport simulation. The first is a line source boundary condition. Along one entire boundary of the 2-D model ($x = 0$), the values of pressure P_0 and concentration C_0 are assigned (line source),

$$\begin{cases} P(x=0) = P_0 & \text{Line pressure source} \\ C(x=0) = C_0 & \text{Line tracer source.} \end{cases} \tag{14}$$

This boundary condition is used to model the situation where the entire borehole is pressurized and injected with tracer. In the second type of boundary condition, the pressure value P_0 is applied at $x = 0$ boundary. But the concentration C_0 is assigned only to a particular location ($z = z_0$) of the boundary,

$$\begin{cases} P(x=0) &= P_0 & \text{Line pressure source} \\ C(x=0) &= \begin{cases} C_0 & z = z_0 \\ 0 & z \neq z_0 \end{cases} & \text{Point tracer source .} \end{cases} \tag{15}$$

The line pressure source will generate fluid flow along the entire $x = 0$ boundary. Therefore, this boundary condition can be used to model the transport in an ambient flow field due to tracer injection at a borehole section. In the third case, the values of pressure P_0 and concentration C_0 are assigned only to particular location $z = z_0$ at the boundary $x = 0$:

$$\begin{cases} P(x=0, z=z_0) &= P_0 & \text{Point pressure source} \\ C(x=0, z=z_0) &= C_0 & \text{Point tracer source .} \end{cases} \tag{16}$$

At the remaining part of the boundary, pressure and concentration are kept at zero,

$$\begin{cases} P(x=0, z \neq z_0) &= 0 \\ C(x=0, z \neq z_0) &= 0 \ . \end{cases} \tag{17}$$

This type of boundary condition can be used to model the situation where a packer is applied to pack a small section of the borehole. Only the packed section is pressurized and injected with tracer. The fourth type of boundary condition is that pressure and tracer concentration are assigned to some point ($z = z_0$) on the boundary $x = 0$. At the remainder of the boundary, the pressure gradient $\partial P/\partial x$ and the concentration gradient $\partial C/\partial x$ are assigned to be zero,

$$\begin{cases} P(x=0, z=z_0) &= P_0 \\ C(x=0, z=z_0) &= C_0 \\ \dfrac{\partial P}{\partial x}\Big|_{(x=0, z\neq z_0)} = 0 \\ \dfrac{\partial C}{\partial x}\Big|_{(x=0, z\neq z_0)} = 0 \ . \end{cases} \tag{18}$$

With the zero gradient boundary condition, the pressure and concentration distributions are symmetric with respect to the $x = 0$ boundary, i.e., $P(-x, z) = P(x, z)$ and $C(-x, z) = C(x, z)$, provided the transport parameters (permeability and porosity) are symmetric about $x = 0$. As we will show, this type of boundary condition can be used to simulate the azimuthal variation of solute transport which is driven by pressure and concentration sources in a vertical borehole.

At the $x = L_x$ boundary, pressure is assumed to be released and a zero pressure is assigned to the boundary. For the concentration, we use the zero gradient boundary condition (i.e., $\partial C/\partial x|_{x=L_x} = 0$). This boundary condition allows non-zero concentration values to be measured at $x = L_x$. At the boundaries $z = 0$ and $z = L_z$, we assume that the medium heterogeneities are repeated periodically with a period of L_z.

Therefore, periodic boundary conditions are used, as given by

$$\begin{cases} P(z=0) = P(z=L_z) \\ C(z=0) = C(z=L_z) \end{cases} . \tag{19}$$

The ADI finite difference solution of Equation (13) for various boundary conditions is given in detail in Appendix A.

SOLUTE TRANSPORT BETWEEN VERTICAL BOREHOLES

In this section, we simulate solute transport in the cross borehole configuration. Two vertical wells are separated by a distance L_x. The formation heterogeneity variation between the wells is assumed to be two-dimensional. A fluid flow field is set up by a borehole pressure P_0 in well A (line or point source). When the steady cross borehole flow is created, tracer is injected into well A, which sets forth tracer transport towards well B. In the simulation, the heterogeneity structure between the two wells is assumed periodic in the vertical direction with a period L_z. Thus the periodic boundary conditions are used at $z = 0$ and $z = L_z$. We will model the solute transport for the line source (Equation 14) and point source (Equations 15 and 16) boundary conditions, respectively.

In the numerical modeling, we use the molecular diffusion coefficient $D_0 = 5 \times 10^{-9}$ m/s^2 (Thompson, 1991; Domenico and Schwartz, 1990). The dispersivity α is a very variable parameter which generally ranges from 1 cm in the laboratory scale to over 10 m in the field scale. Therefore, in our simulation of a field situation (the model dimension is on the order of 127 m), we use $\alpha = 10$ m. Tracer concentration is scaled to 1 at the boundary ($C_0 = 1$) and the borehole pressure P_0 is taken as 1 MPa. Permeability and porosity are varied for each individual case.

Homogeneous Medium

In this section we use the 1-D analytical solution for the solute transport in the homogeneous medium to examine the effects of various transport parameters, such as, D_0, α, and fluid velocity U. We also use the 1-D solution to check the accuracy of our finite difference algorithm.

The analytical solution for Equation (9) in an infinite 1-D homogeneous medium is given by (Domenico and Schwartz, 1990)

$$\frac{C(x,t)}{C_0} = \frac{1}{2}\left[erfc\left(\frac{x-Ut}{2\sqrt{Dt}}\right) + exp\left(\frac{Ux}{D}\right) ercf\left(\frac{x+Ut}{2\sqrt{Dt}}\right)\right] . \tag{20}$$

Using this equation, we can examine the effects of parameters D_0, α, and U on the solute mass transport. Figure 1 shows the tracer concentration *vs.* distance x for three different D_0 values. They are $D_0 = 5$, 50, and 500 $\times 10^{-5}$ cm^2/sec, respectively. In this figure, α and U are fixed at 25 cm and 9.2 $\times 10^{-5}$ cm/sec, and the curves are evaluated

at the time of 24 hours after the tracer injection at $x = 0$. From this figure, we can see that increasing D_0 increases the tracer diffusion into the medium. However, D_0 only moderately affects the transport process, as the three curves change only moderately over a two order of magnitude change of D_0 (5×10^{-5}cm^2/sec to 500×10^{-5}cm^2/sec).

In Figure 2, the effects of dispersivity α are studied. In this case, D_0 and U are kept constant ($D_0 = 5 \times 10^{-5}$cm^2/sec and $U = 9.2 \times 10^{-5}$cm/sec respectively). The recording time is the same as in Figure 1. The dispersivity α is varied from 5 cm to 50 cm. From this figure, we can see that α significantly influences the solute concentration distribution. The front of the solute concentration curve becomes flat with increasing α values, showing that the solute mass disperses with increasing dispersivity α.

The effects of fluid flow velocity U are illustrated in Figure 3. In this figure, we set $\alpha = 5$ cm, $D_0 = 5 \times 10^{-5}$cm^2/sec, U is varied from 9.2 to 920 $\times 10^{-5}$ cm/sec, the recording time is set at t = 1.2 hours. For small flow velocity (9.2 $\times 10^{-5}$ cm/sec), the solute front is moved only a small distance into the medium (solid curve) and this solute migration is largely due to diffusion (see Figure 3). However, when the velocity is increased to 920 $\times 10^{-5}$ cm/sec, the tracer front is effectively carried away by the fluid flow into the medium. At the same time, the solute mass becomes significantly dispersed, because of the dispersion term expressed as the product αU in the tracer transport equation.

We now compare our finite difference modeling results with the result of the analytical solution given in Equation (20). In finite difference modeling, we set the 2-D model size $L_x = L_z = 127$ cm, the molecular diffusion coefficient $D_0 = 5 \times 10^{-5} cm^2/s$, dispersivity $\alpha = 25$ cm, and the effective velocity $U = 9.2 \times 10^{-5}$ cm/s. Figure 4 shows the comparison between the analytical solution (Equation 20) and the finite difference solution for the profile along $z = L_z/2$ at t = 1.87 hours and 23.39 hours. In this homogeneous medium case, the finite difference results agree almost exactly with the analytical solution.

Next, we use the homogeneous medium to demonstrate the effect of source dimension on the shape of the solute plume. The model parameters we used here are $L_z = L_x = 127$ m. The molecular diffusion coefficient is $D_0 = 5 \times 10^{-9}$ m^2/sec, and the dispersivity $\alpha = 5$ m. Figure 5 shows the solute concentration contours at $t \approx 17.64$ hours for a line pressure source of 1 MPa and a line concentration source of 1 (normalized intensity) at $x = 0$ boundary. For the homogeneous medium, the contours are straight lines parallel to the $x = 0$ boundary. The solute concentration contours correspond to the dispersed advective front of the solute plume.

For the same line pressure source and a point concentration source (Equation 15), Figure 6 shows the concentration contours at $t \approx 1.47$ days. All the parameters used in this modeling are the same as those used in Figure 5. As seen from this figure, the solute plume shows significant elongation along the flow direction. The closer to the source region, the denser the contours. This behavior is very different from the line source case shown in Figure 5. The lateral spreading of the concentration contours reflects the effects of diffusion and dispersion of the solute transport, while the longitudinal elongation of the contours reflects the advection effects due to the velocity field, which

is a constant vector pointing to the x-direction.

For the point pressure ($P_0 = 1$ MPa) and point concentration sources (Equation 16), the elongation of the concentration contours almost vanishes except in regions very close to the source. The lateral spreading is very significant (Figure 7). The reason for this is that the velocity field generated by the point pressure source spreads almost radially and vanishes away from the source. At large distances away from the source boundary, the solute concentration distribution is almost isotropic. These model examples with different pressure and concentration sources show that the solute transport depends strongly on the source dimension as well as boundary conditions.

Random Permeability

For the heterogeneous medium cases, we first simulate the solute transport in a formation with random permeability variations. Figure 8 shows the random permeability distribution (image). The model size is 127 m $\times$ 127 m. The permeability field is generated by convolving a 2-D random field using a 2-D Gaussian correlation function with a correlation length of 5 m (see Zhao and Toksöz, 1991). This random permeability field has a mean of 1 Darcy and standard deviation of 25%.

• **Line source** We first use the line source boundary conditions (Equation 14) for the simulation. The pressure contours are also shown in Figure 8 for the line pressure source (solid curves). The pressure field is calculated by applying a constant pressure of 1 MPa at $x = 0$ boundary. The corresponding flow velocity field is calculated using Equations (11) and (12). The simulated mass solute plume at times 7.06 and 28.22 hours are shown in Figure 9. Comparing the solute concentration distribution with the pressure distribution (the contours in Figure 8), we see that the solute concentration is more sensitive to the permeability heterogeneity than the pressure field. This happens because the advection of the solute mass flux is determined by the velocity field, which results from the spatial differentiation of the pressure field (Equations 11 and 12). The tortuous flow field results in the undulating shape of the plume. At a later time, the solute concentration distribution in the near source region tends to become homogeneous. The physical explanation for this phenomenon is that, after the breakthrough by the solute mass, the diffusion effects in the solute transport tend to make the solute concentration homogenized, even for low permeability regions.

In the next model, the permeability distribution is lineated at a 45^o angle from the x direction. The correlation lengths of the random field are 20 m in the lineation direction and 2 m perpendicular to this direction. Figure 10 shows the lineated permeability distribution (image), which has the same mean and standard deviation as the isotropic distribution in Figure 8. The pressure contours for this permeability distribution are also plotted in Figure 10 (solid curves). The solute concentration contours for the line pressure and line tracer sources are shown in Figure 11 for the early time (7.06 hours, upper figure) and for the late time (28.22 hours, lower figure). For the late time, in regions where strong advection and dispersion occur (dense contour curves), the concentration contours are significantly modulated by the permeability lineation.

The solute mass moves farther along the lineated high permeability regions than along the low permeability regions, resulting also in the lineation of the concentration distribution. In the near source region, concentration values in low and high permeability regions tend to become homogenized, because of the diffusion effects.

• **Point source** We now show the modeling results for the line pressure and point tracer source (Equation 15) boundary conditions. Figure 12 shows the simulated concentration contours for the lineated random Gaussian model at time steps 0.88 days (upper figure) and 8.82 days (lower figure). The concentration contours originate from the point tracer source and are elongated towards the direction of pressure gradient (45^o to the x-direction). The modulation due to directional (or lineated)permeability is clearly seen in the central part of the plume, which is similar to the line source case in Figure 11. Away from the axial regions the concentration contours are less sensitive to the directional permeability, because of the lateral spreading and diffusion of the solute transport.

The case of point pressure ($P_0 = 1$ MPa) and point concentration ($C_0 = 1$) boundary conditions is shown in Figure 13 for the same time steps. Only in the near source region do the concentration contours show some modulation due to the lineation of permeability. Away from the source, the amplitude of the advection velocity field quickly decreases with distance, and the diffusion and dispersion become dominant, which results in the decreasing of the permeability lineation effects. Therefore, for this case, the effect of directional permeability on the solute transport is insignificant away from the source region.

The simulation of solute transport in random, continuous permeability media shows that the solute transport is sensitive to the medium permeability and/or porosity structure and that the contouring of the solute concentration can help delineate the medium heterogeneities, if the tracer transport occurs in a broad ambient background. For localized flow field (point pressure source), the effect of permeability heterogeneity is significant mainly in the near source region (i.e., the point pressure and point tracer sources case).

Random Flow Channel Model

In many reservoirs, layered structures are severely distorted by geological movements such as faulting, layering, *etc.*. As a result, the reservoir connectivity condition may have been altered or destroyed. We model this situation using the random flow channel model shown in Figure 14. This model is made from the aligned permeability (porosity) model of Figure 10 (at 0^o lineation direction). A threshold of 60% of the maximum permeability (porosity) is used. Regions in which the permeability (porosity) exceeds the threshold are kept unchanged, while regions whose permeability (porosity) is below the threshold are assigned very small permeability (porosity) values (about 1/200 of the maximum value) (see also Zhao and Toksöz, 1991). As a result, the inter-well permeability (porosity) connectivity is greatly reduced. The two wells are connected only through high permeability channels at z = 0 - 12 m and 94 - 99 m. Other permeability

channels terminate inside the formation.

We present the results of solute transport simulation for the model shown in Figure 14. The boundary conditions are those of the line pressure and solute (Equation. 14). The contours in Figure 14 are the pressure field calculated for the model. For the solute transport modeling, the parameters used are the same as in the previous modelings. Figure 15 shows the solute concentration distribution at times of 14.12 hours and 2.94 days respectively. At an early time (the upper figure in Figure 15), the solute transport primarily occurs along the permeability channels that are connected with the source well. As time increases, more solute mass diffuses into the low-permeability regions although the solute mass is still concentrated in the high-permeability regions. The breakthrough of the solute mass at well B occurs at two major flow channels that connect the two wells.

We now show the simulation for the line pressure, point tracer source boundary conditions. The tracer source is placed at the $x = 0$ boundary in the flow channel at $z = 95 - 98$ m, which connects the two wells, and at $z = 55 - 58$ m, which extends towards well B, but terminates at about 50 meters from well B. The tracer plumes at 5.88 days for the two cases are shown in Figure 16. In the upper figure of Figure 16, because the flow channel connects the two wells, solute mass moves from well A to well B with ease, although a portion diffuses outside of the channel. For the lower figure in Figure 16, solute mass moves fast with flow until it meets the channel end; afterwards, the solute transport moves into the formation in the form of diffusion. The front of the solute concentration contour from then on changes from a flat to a round shape.

Figure 17 shows the solute concentration measured at two locations in the flow channel model. One is at $x = 90$ m and $z = 98$ m, which is in the major flow channel that connects the two wells. The other location is at $x = 90$ m and $z = 57$ m, which is close to the flow channel that terminated at about 50 m from well B. At early times ($t < 100$ hours), the concentration in the connected channel increases quickly, while the concentration outside the terminated flow channel is very small. The latter concentration then increases with time because of the solute mass diffusion into the low-permeability region.

The modeling results of Figures 16 and 17 demonstrate that although tracers can be detected at various parts of the receiver well because of diffusion effects, the connectivity of the reservoir in terms of flow is manifested by a high level of tracer concentration, which provides a method for measuring cross borehole connectivity using tracer measurements.

Permeable and Impermeable Layer Sequences

An important application of solute transport in reservoir characterization is the tracer test to study the inter-well reservoir connectivity, particularly when the formation has a layered structure. To simulate solute transport in these situations, the layered permeability structure is used, as shown in Figure 18. The permeabilities of the high and low permeability layers are 1 and 0.01 Darcy, respectively. These layers are generated

using the Poisson process. That is, the average thickness of the layers is 4 m, the distribution of the layer thickness obeys the Poisson distribution (see Zhao and Toksöz, 1991). The lower figure in Figure 18 is the simulated fluid flow field for a line pressure source $P_0 = 1$ MPa at the $x = 0$ boundary. The flow field clearly reflects the high or low permeability layers.

The solute concentration distribution at time steps 14.12 hours and 2.94 days are simulated in Figure 19 for the line pressure and line tracer sources. The channeling of the solute transport by the high permeability layers is best illustrated by the layered structure. Because the fluid flow velocity in permeable layers is by an order of magnitude larger than that in the low permeability layers, the solute transport occurs primarily along the permeable layers. Consequently, the impermeable layers become low-concentration layers. In this case, if the concentration can be measured along well B, the low and high values of concentration will allow permeable and impermeable channels to be mapped. In fact, this is the basis for studying inter-well reservoir connectivity by means of cross-borehole tracer tests.

However, it is worthwhile to point out that, in the case of a thin impermeable layer sandwiched between two major permeable layers, the diffusion effect will allow solute transport to penetrate the thin layer, even though the layer has very low permeability. This is evident by inspecting the concentration contour around $z = 30$ m, where the impermeable layer affects the contour shape only slightly. Also, comparing the concentration distribution at $t = 14.12$ hours with that at $t = 2.94$ days, some of the obvious low-concentration channels at $t = 14.12$ hours become less visible at $t = 2.94$ days, because of the increase of concentration with time as a result of the diffusion into the layers. Figure 20 shows the solute mass image at t = 5.88 days when the solute mass breakthrough occurs in well B.

To explain the diffusion effects, we model the solute transport due to a point tracer source through a high permeability and porosity channel of thickness of 10 m (Figure 21) embedded in a low permeability and porosity background. The permeability and porosity values are 1 Darcy and 0.2 in the channels and 0.01 and 0.002 in the background. The fluid flow field would be largely confined in the permeable layer. The concentration contours at t = 14.12 hours and 5.88 days are shown in Figure 22. Although solute mass is very effectively carried forward by the fluid flow along the high permeability channel, a portion of solute mass diffuses into the low-permeability background. The localizing mass in the high permeability channel provides the opportunity for large concentration gradients to develop (see Figure 22). Therefore, with increasing time, a significant portion of solute mass will enter into the surrounding medium.

Returning to Figure 20, we see that the concentration image at t = 5.88 days shows the significant smearing due to diffusion; some impermeable layers in the original model (the upper figure in Figure 18) become less visible in the concentration image. The implication of this example for the field tracer test is that some thin impermeable layers may not be seen in the tracer measurements, because of the diffusion effect.

AZIMUTHAL VARIATIONS OF SOLUTE TRANSPORT FROM A SINGLE BOREHOLE

In this section, we model the solute transport in a horizontal plane due to a pressure and a tracer source in a single well. Many solute transport problems can be modeled in this way. For example, in reservoir or ground water problems, the vertical extent of the reservoir or water aquifer is considerably smaller than its horizontal dimension. Thus, the 2-D configuration is a good approximation. The azimuthal variation of a tracer concentration in such a case is an important means to detect reservoir connectivity and fluid movement, and permeability anisotropy.

We use the boundary condition for the symmetric point source (Equation 18) to model solute transport. If we assume that the permeability and porosity distributions are symmetric about the $x = 0$ boundary, the boundary condition $\partial P/\partial x = 0$ and $\partial C/\partial x = 0$ then imply that the pressure and concentration distributions are also symmetric with respect to the $x = 0$ boundary. Therefore, by flipping the simulation results over to $x < 0$ domain, the solute transport will resemble that of a point source. In this way, we can use the formulation in the Cartesian coordinates to model solute transport from a point source, which would otherwise require a more complicated formulation in the cylindrical coordinates. This approach would be adequate if we wish to model the anisotropic transport along different directions in the horizontal plane, which is due to the anisotropic distribution of permeabilities (such as lineated permeabilities, fractures, *etc.*). To demonstrate the validity of this approach, Figure 23 shows the solute transport for a homogeneous permeability (1 Darcy) and porosity (0.2) calculated using the symmetric point pressure ($P_0 = 1$ MPa) and tracer ($C_0 = 1$) source boundary conditions. The concentration contours at the left side of the source are obtained by flipping those at the right side of the source over to the left. The contours are shown for $t = 8.82$ days. The concentration contours are concentric circles around the source, as would be expected for transport from a cylindrical symmetric source.

The effects of formation heterogeneity are now studied. We first use a lineated permeability (porosity) variation model generated using the aligned Gaussian correlation function (correlation lengths are $a_1 = 20$ m and $a_2 = 2$ m, respectively, see Zhao and Toksöz, 1991). The average permeability (porosity) is 1 Darcy (0.2), and the standard deviation is 28%. Figure 24 shows the permeability distribution (image) and the simulated pressure field (solid curves). Figure 25 shows the solute mass concentration for the model shown in Figure 24. The effects of permeability lineation on the anisotropic behavior of tracer transport can be observed. Although the local tracer concentration is clearly modulated by the permeability lineation, the overall feature of the tracer concentration contours does not differ greatly from that of the homogeneous permeability results in Figure 23. Thus the lineation of continuous permeability heterogeneity does not produce significant anisotropy in the tracer transport. We notice that in the near source region the tracer concentration is saturated because of the diffusion effects, as discussed previously.

We study next the effects of the discontinuous permeability (porosity) model. The same discontinuous model as in Figure 18 (upper figure) is used for the permeability

(porosity) heterogeneities. The location of the well is indicated by a dot in a high permeability (porosity) layer in this model (Figure 26). Figure 27 shows the simulated solute mass concentration contours for the model of Figure 26 due to a pressure of 1 MPa and a unit tracer concentration ($C_0 = 1$) in the well. The contours are shown for the time of 2.94 days (upper figure) and 11.76 days (lower figure). Because the fluid flow is largely confined in the high permeability (porosity) layers, the solute mass is effectively moved in the lineation direction of the layers. As time increases, the tracer can also enter the low permeability layer due to diffusion. Nevertheless, the anisotropy in the tracer concentration distribution is very significant for the layering model. Therefore, the discontinuous heterogeneity models can produce significant anisotropic effects in the tracer transport.

As a final example, we study the anisotropy effects of tracer transport due to a permeable flow channel that intersects the borehole. In the field situation this flow channel may represent a vertically fractured zone generated by borehole hydraulic fracturing treatment. The determination of the direction and extension of the fracture zone in the formation is an important issue in hydro-fracturing applications.

We simulate the fracture zone as a high permeability (1 Darcy) and porosity (0.2) channel of 2 m in a low permeability (0.01 Darcy) and porosity (0.002) background. Figure 28 shows the configuration of the channel. The source well is located at the center of the channel and three receiver wells (A, B, and C) are located at 40 m away from the source. The angular directions are 0^o, 45^o, and 90^o measured along the extension direction of the channel (Figure 28). The source to channel end distance is 35 m. A pressure source of 1 Mpa and tracer source ($C_0 = 1$) is applied at the source well. Figure 29 shows the simulated tracer concentration contours for the time of 1.18 days from the tracer injection. As expected, the tracer concentration shows a quasi-elliptical shape. The elongation in the channel direction is due to the fluid movement along the channel while the tracer movement perpendicular to the channel is due to the diffusion effects. The tracer-time history measured at the three receiver wells is plotted using the semi-logarithmic plot in Figure 30. The concentration along the channel direction is the greatest; it decreases as the angle of the source-receiver well direction increases, showing strong anisotropy. The anisotropy is the greatest at the early time, and decreases with time because of the increase of tracer concentration due to diffusion. This example suggests that it is possible to determine the hydro-fracture orientation in the formation by measuring the anisotropy effects in the tracer test.

CONCLUSIONS

In this study, we have numerically investigated the behavior of solute mass transport in heterogeneous media with emphasis on the effects of permeability heterogeneities. Basically, there are two fundamental mechanisms that control the transport process, diffusion and advection. The dispersion effect contributes to the diffusion or mechanical mixing on the transport process because of the fluid advection. Therefore, in a medium with fluid flow, the solute transport is largely carried out by fluid advection, and modified by the diffusion process. The dependence of solute transport on fluid advection

makes tracer experiments an important means for analyzing medium permeability heterogeneity. However, the resolution of heterogeneity may be smeared by the diffusion effect because solute mass can also be moved into low permeability regions through the diffusion process.

Because the solute transport is largely controlled by fluid advection, the dimension of the pressure source that drives the fluid advection controls the tracer distribution, in addition to the dimension of the tracer source. The effects of the source dimension have been demonstrated in our numerical simulation.

The effects of permeability heterogeneity were studied by using various permeability distributions which are characterized as continuous and discontinuous models (see Zhao and Toksöz, 1991). For the continuous distribution models, our numerical simulations show that the tracer distribution is distorted by the local variation of permeability, but the global behavior of the distribution still resembles that of the homogeneous distribution. Significant effects are found from the discontinuous permeability models, where fluid advection takes place largely within high permeability flow channels. As a result, the tracer transport is effectively carried away along these channels. This offers effective means for characterizing reservoir connectivity and permeability anisotropy through tracer experiments. An important phenomenon in the tracer transport in the discontinuous permeability media is that thin low permeability flow barriers may not be detected by the tracer experiment because the diffusion process can move the solute mass into the low-permeability regions. This has been demonstrated by our numerical modeling examples. Therefore, in characterizing reservoir heterogeneities using tracer experiments, one should be aware of the smearing effects due to the diffusion process.

We have also shown that lineation permeability can result in anisotropic behavior in the tracer transport. However, the anisotropy is small if the permeability heterogeneity variation is continuous. Significant anisotropic effects exist when the permeability variation is discontinuous. The anisotropic effects in the tracer transport can be used to infer the orientation of fractures and/or permeable channels.

ACKNOWLEDGEMENTS

This research was supported by the Borehole Acoustics and Logging Consortium at M.I.T. and by Department of Energy Grant DE-FG02-86ER13636.

REFERENCES

Domenico, P.A. and F.W. Schwartz, 1990, *Physical and Chemical Hydrogeology*, Wiley, 605 3rd Ave., NY.

Ferziger, J.H., 1981, *Numerical Methods for Engineering Applications*, John Wiley & Sons, Inc., New York, 1981.

Grisak, G.E. and J.F. Pickens, 1980, Solute transport through fractured media, 1, The

effect of matrix diffusion, *Water Resour. Res., 16(4)*, 719–730.

Moreno, L., Y.W. Tsang, C.F. Tsang, F.V. Hale, and I. Neretnieks, 1988, Flow and tracer transport in a single fracture: A stochastic model and its relation to some field observations, *Water Resour. Res., 24(12)*, 2033–2048.

Raven, K. and K.S. Novakowski, 1984, Field investigation of the solute transport properties of fractures in monzonific gneiss, *Internat. Symposium on Groundwater Resources Utilization and Contaminant Hydrogeology*, Vol. II: Pinawa, Manitoba, Atomic Energy of Canada Ltd., 507–516.

Tang, D.H., E.O. Frind, and E.A. Sudicky, 1981, Contaminant transport in fractured porous media: Analytical solution for a single fracture, *Water Resour. Res., 17(3)*, 555–564.

Thompson, M.E., Numerical simulation of solute transport in rough fractures, 1991, *J. Geophys. Res., 96*, 4157–4166.

Tsang, Y.W., C.F. Tsang, I. Neretnieks, and L. Moreno, 1988, Flow and tracer transport in fractured media: A variable aperture channel model and its properties, *Water Resour. Res., 24(12)*, 2049–2060.

Zhao, X.M. and M.N. Toksöz, 1991, Modeling fluid flow in heterogeneous and ansotropic porous media, *M.I.T. Full Waveform Acoustic Logging Consortium*, 245–270.

Zhao, X.M. and M.N. Toksöz, 1992, Transient fluid flow in heterogeneous porous media, *M.I.T. Borehole Acoustics and Logging Consortium*, 131–156.

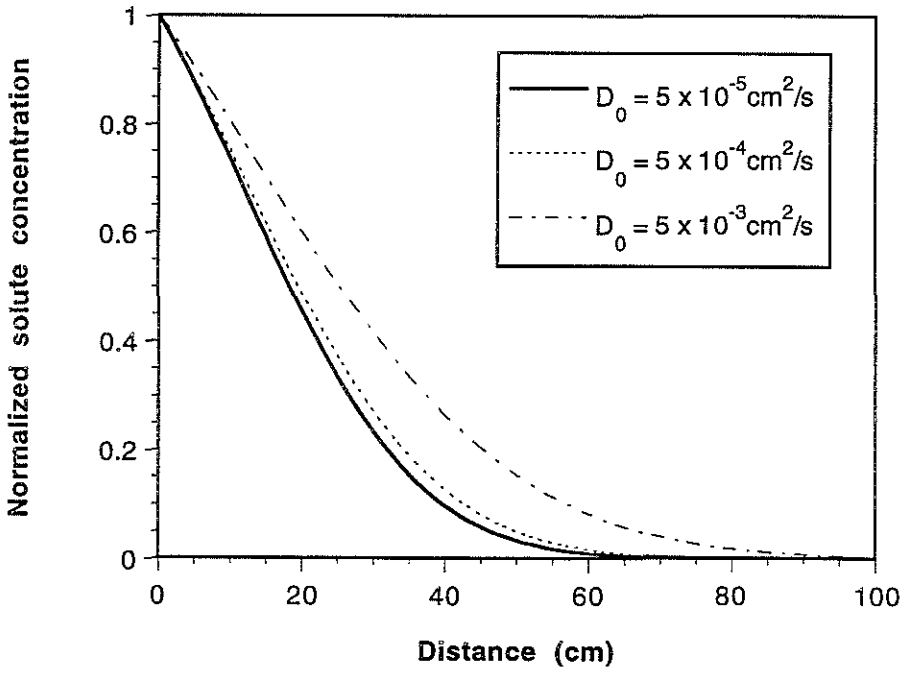

Figure 1: Analytical solution for different D_0 values.

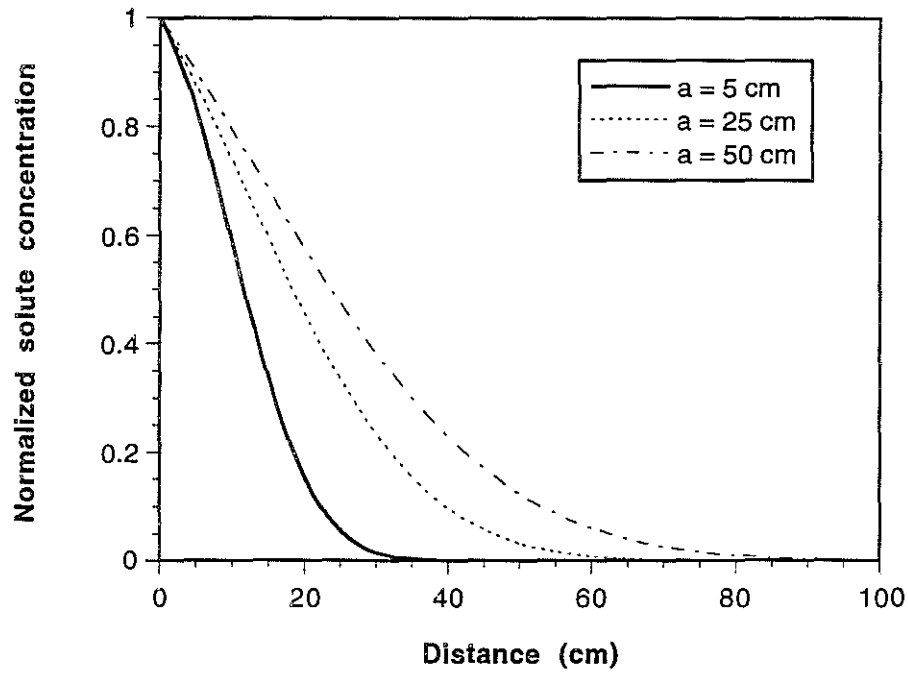

Figure 2: Analytical solution for different α values.

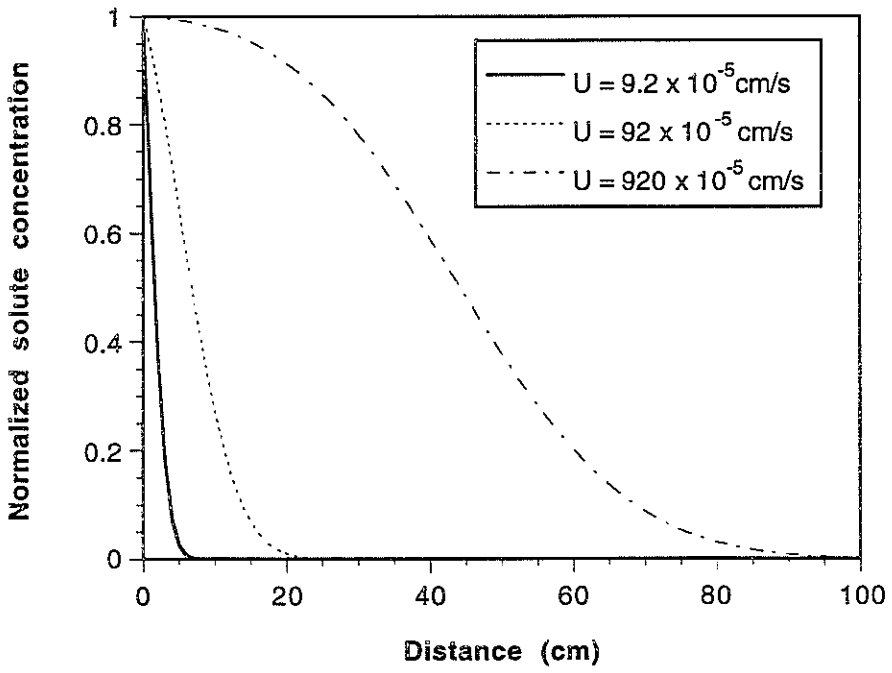

Figure 3: Analytical solution for different U values.

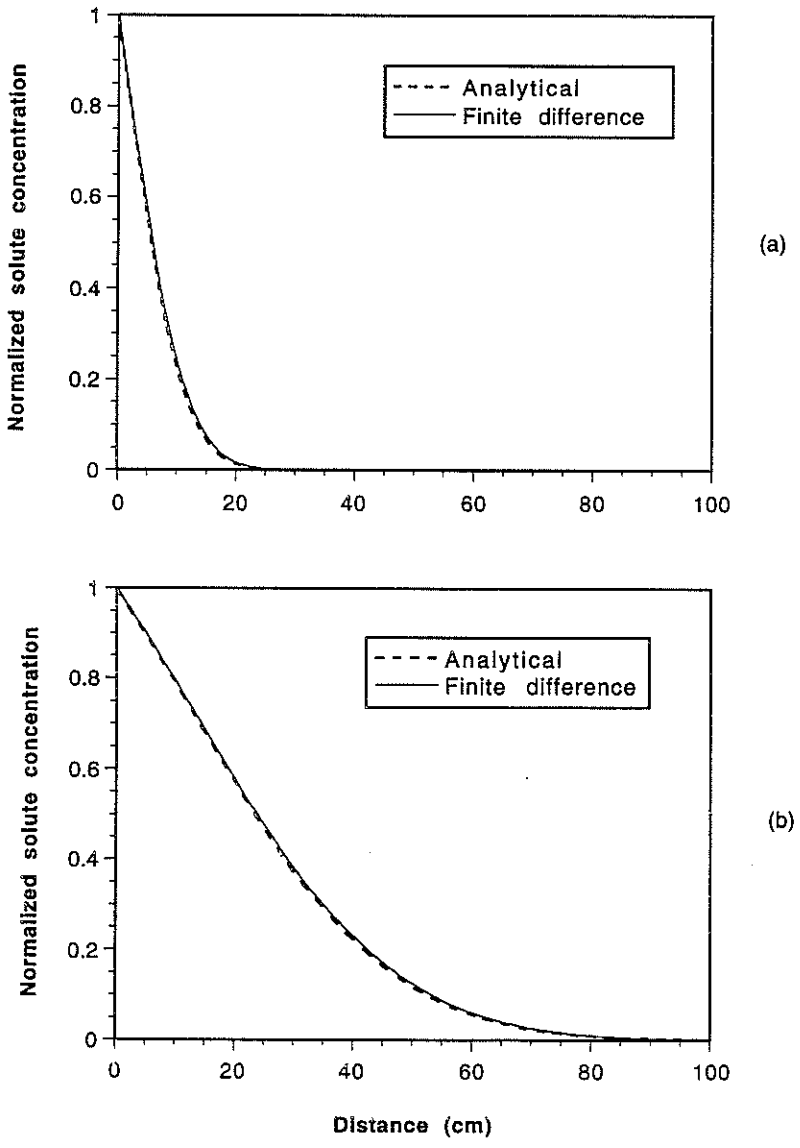

Figure 4: Comparison of analytical solution and finite difference modeling results at (a) 1.87 hours and (b) 23.39 hours for velocity $U = 9.2 \times 10^{-5}$ cm/sec, $D_0 = 5 \times 10^{-5}$ cm^2/sec, and $\alpha = 25$ cm.

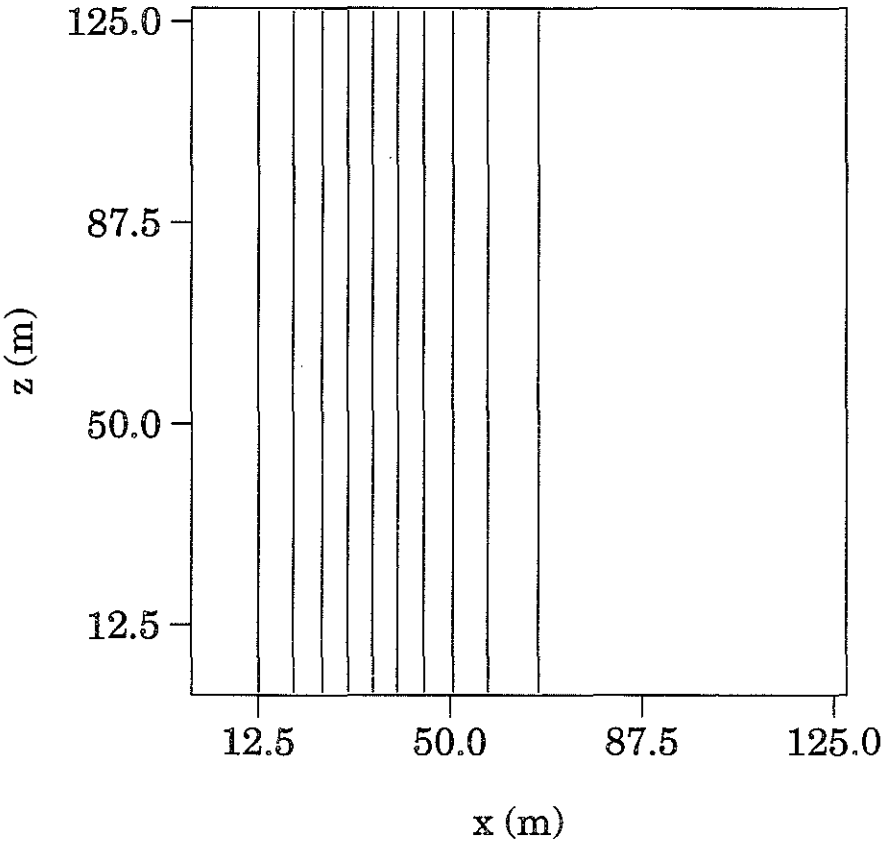

Figure 5: Solute concentration contours at $t \approx 17.64$ hours for a homogeneous medium, line pressure, and concentration sources.

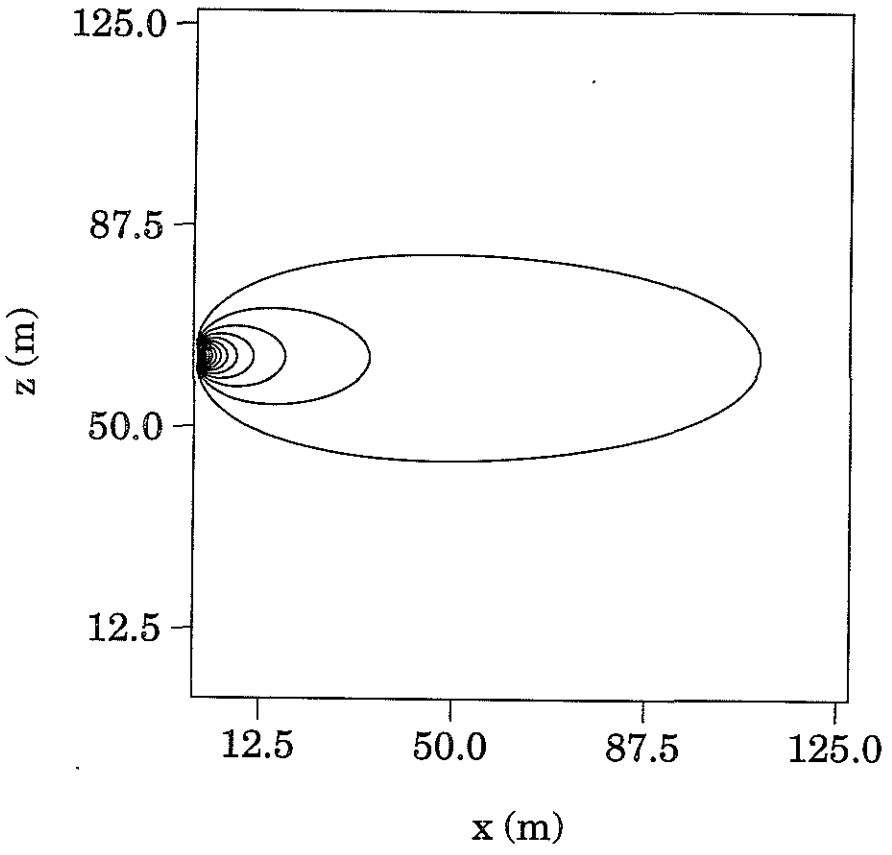

Figure 6: Solute concentration contours at $t \approx 1.47$ days for a homogeneous medium, line pressure source, and point concentration source.

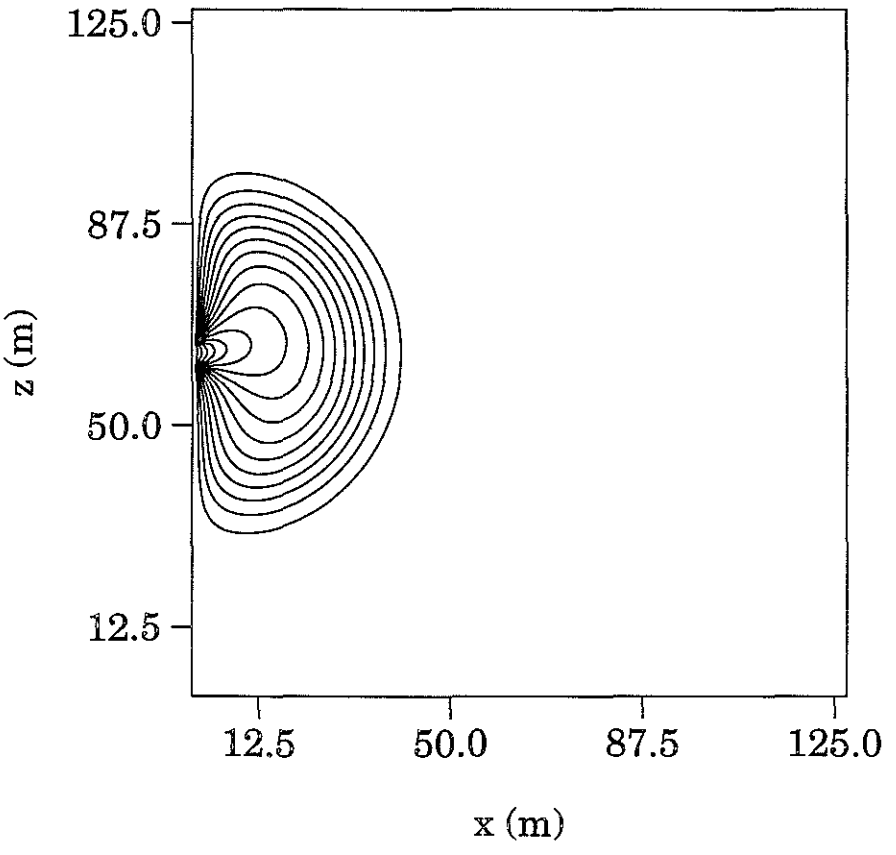

Figure 7: Solute concentration contours at $t = 1.18$ days for point pressure tracer sources.

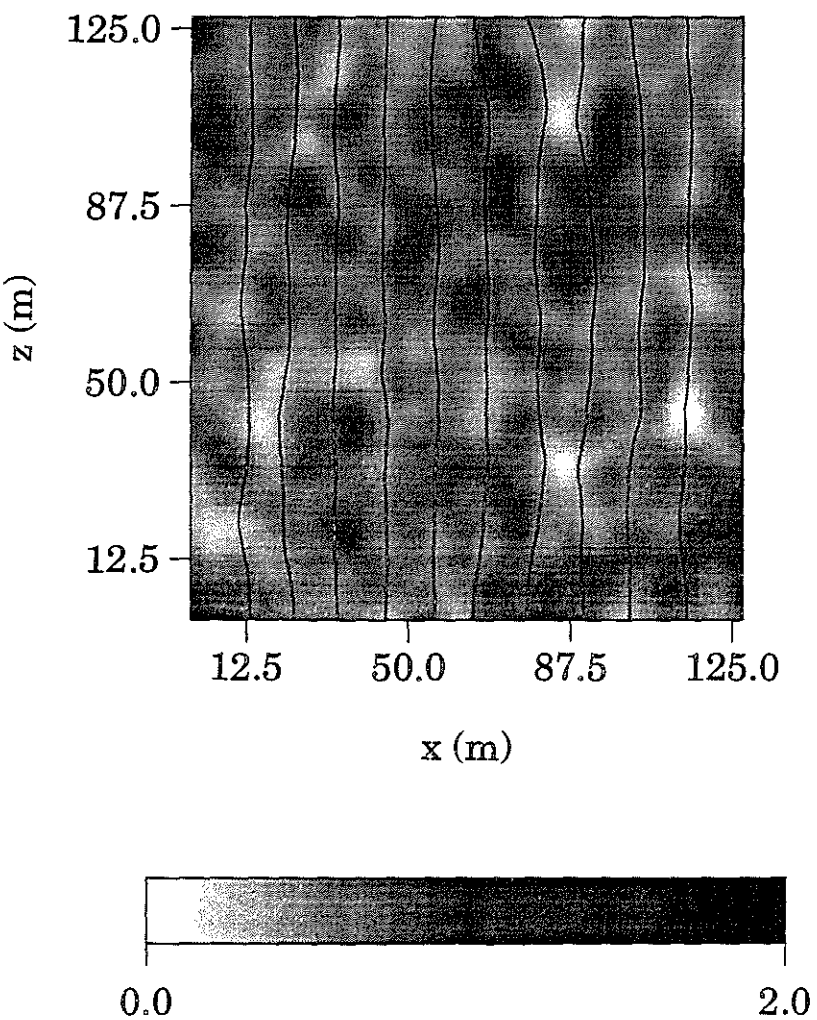

Figure 8: Gaussian random permeability distribution with $a_1 = a_2 = 5$ m and simulated pressure fields (contours). The model dimensions are 128 × 128 m.

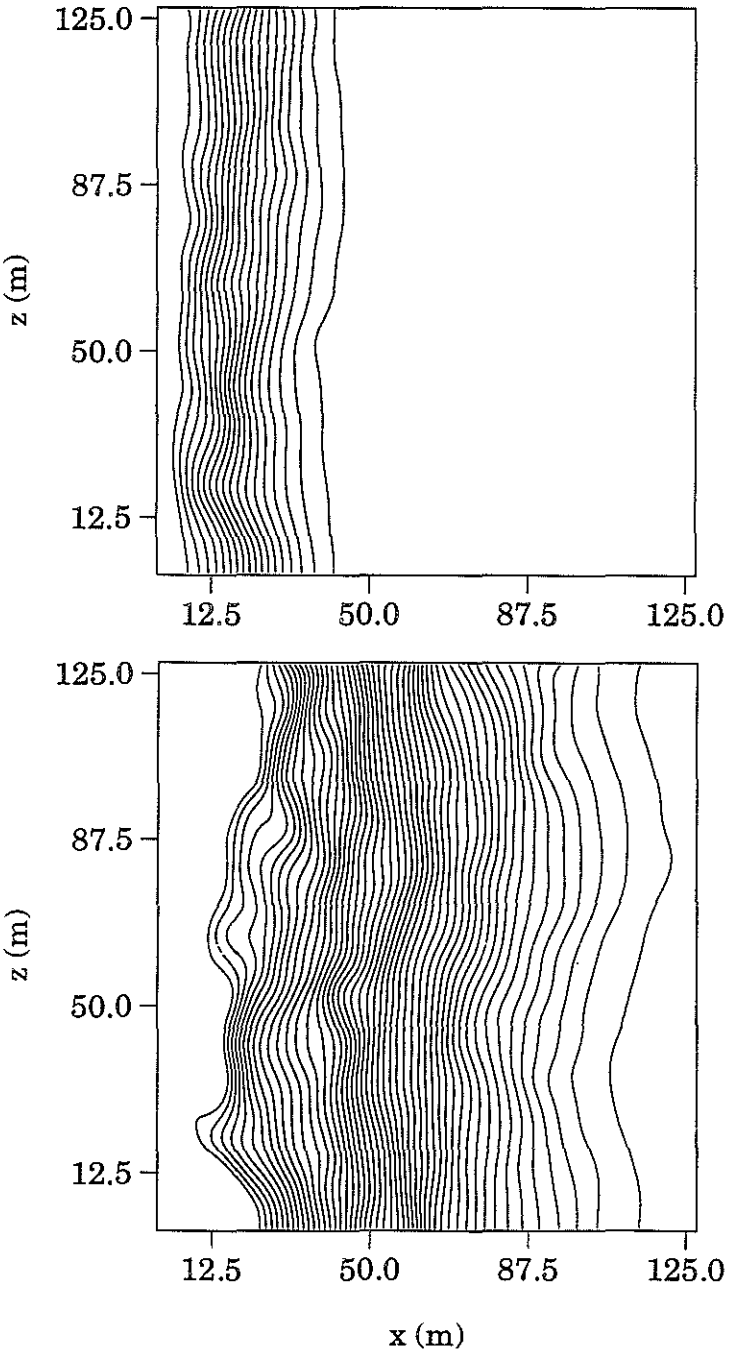

Figure 9: Solute concentration contours for Gaussian permeability distribution shown in Figure 8. The upper figure shows the concentration contours at $t \approx 7.06$ hours, the lower one at $t \approx 28.22$ hours.

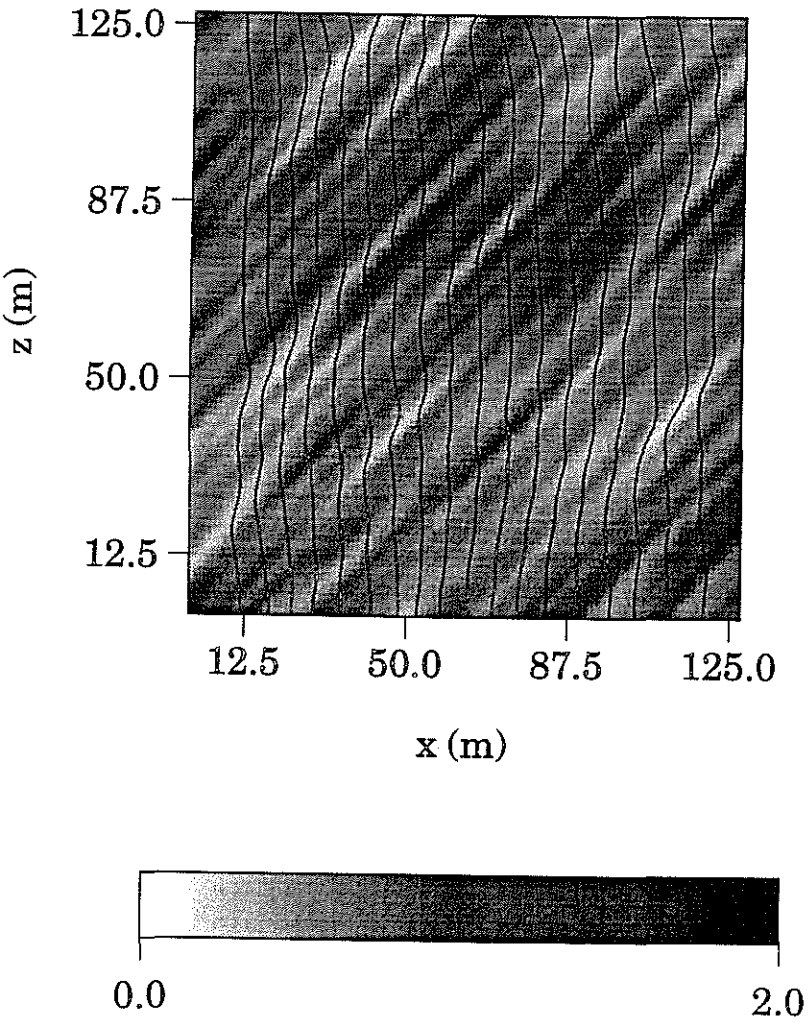

Figure 10: Aligned Gaussian random permeability distribution with $a_1 = 20$ m, $a_2 = 2$ m, model size of 128 m. The simulated pressure field is also plotted (the contours).

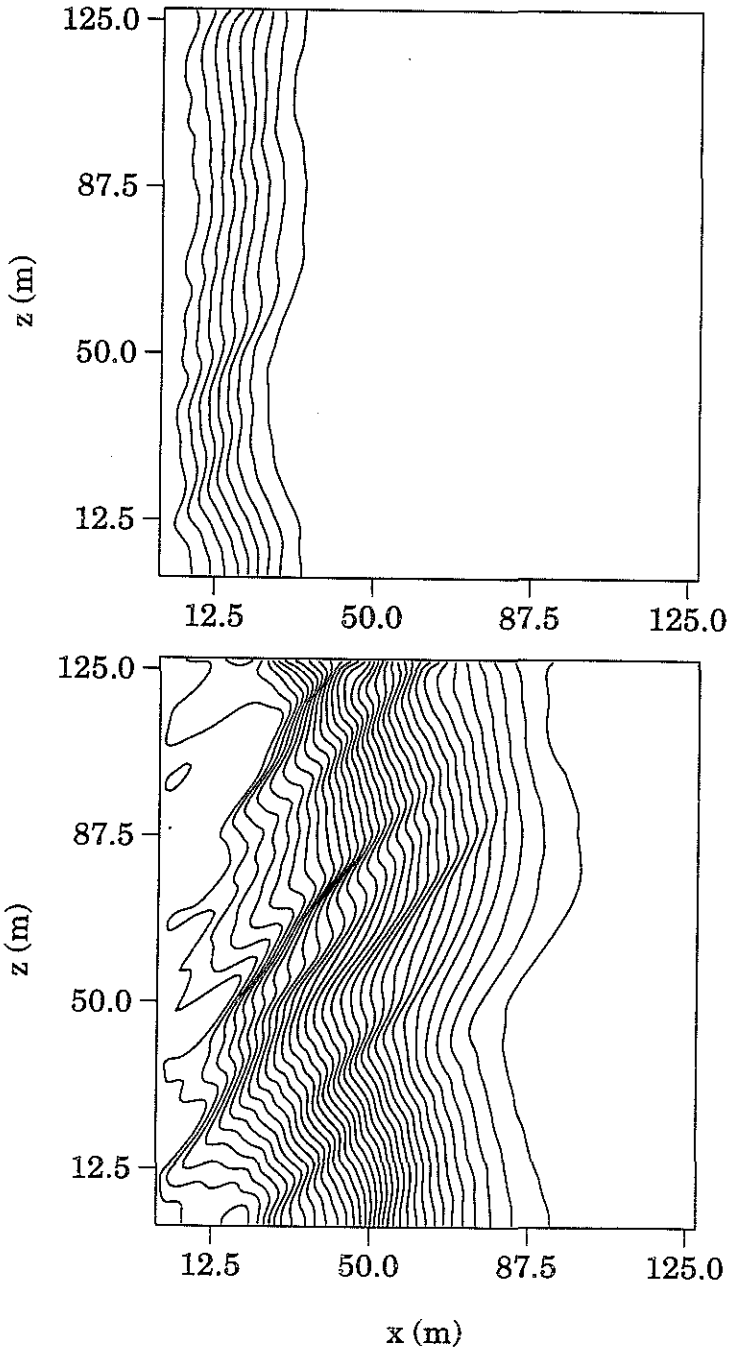

Figure 11: Solute concentration contours for Gaussian permeability distribution shown in Figure 10 and line pressure, line tracer source. The upper figure is the concentration contour at $t \approx 7.06$ hours, the lower one is at $t \approx 28.22$ hours.

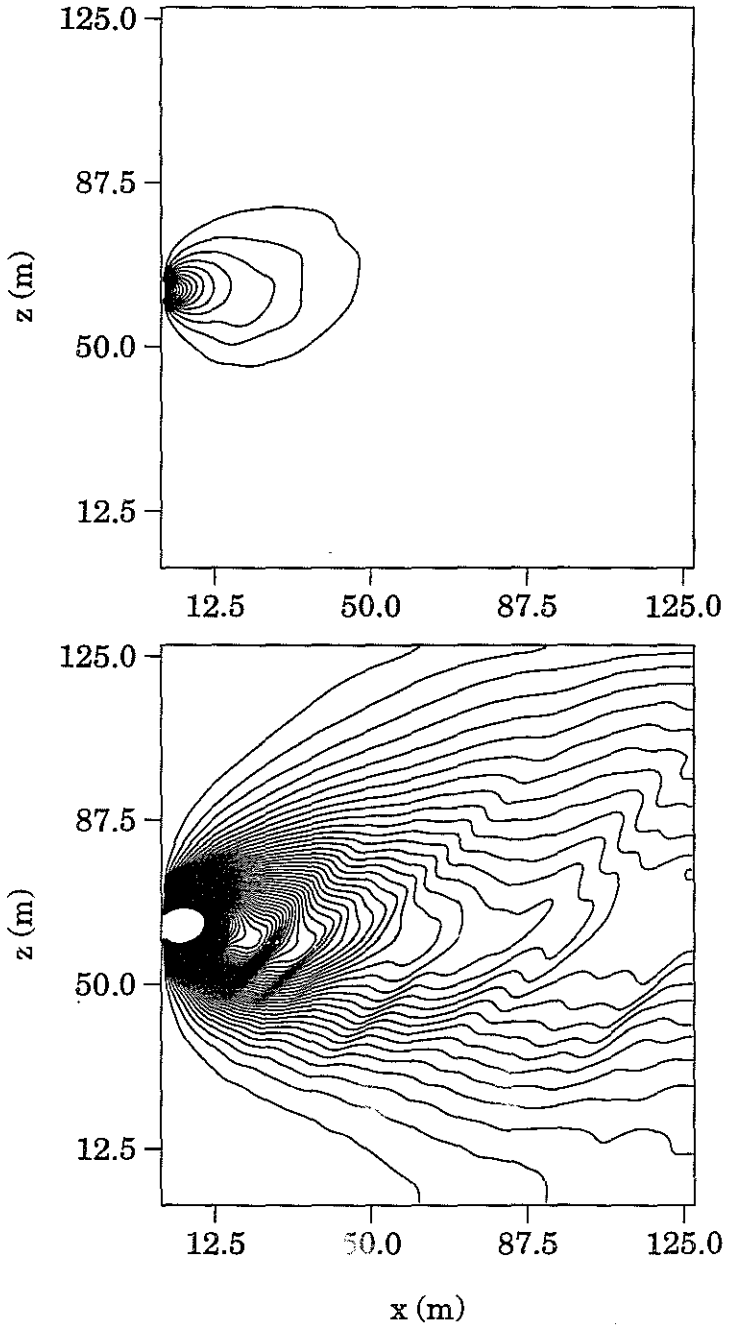

Figure 12: Solute concentration contours for the aligned Gaussian permeability distribution shown in Figure 10 and line pressure, point tracer source. The upper figure is the concentration contour at $t \approx 0.88$ days, the lower one is at $t \approx 8.82$ days.

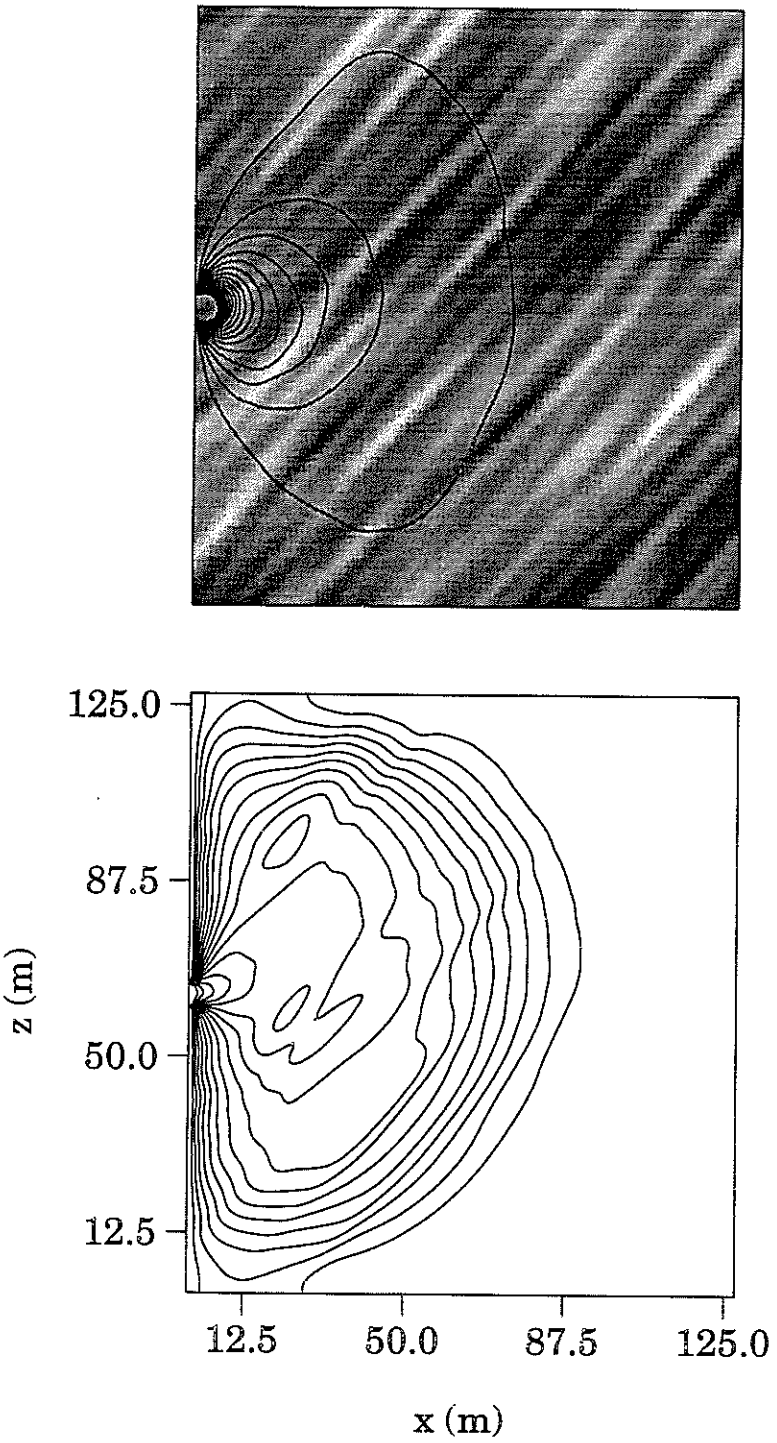

Figure 13: Simulated results for the aligned Gaussian random permeability distribution (same as Figure 20) for point pressure and point tracer sources. The upper figure is the permeability image with the pressure contours. The lower figure is the solute concentration contours at $t = 8.82$ days.

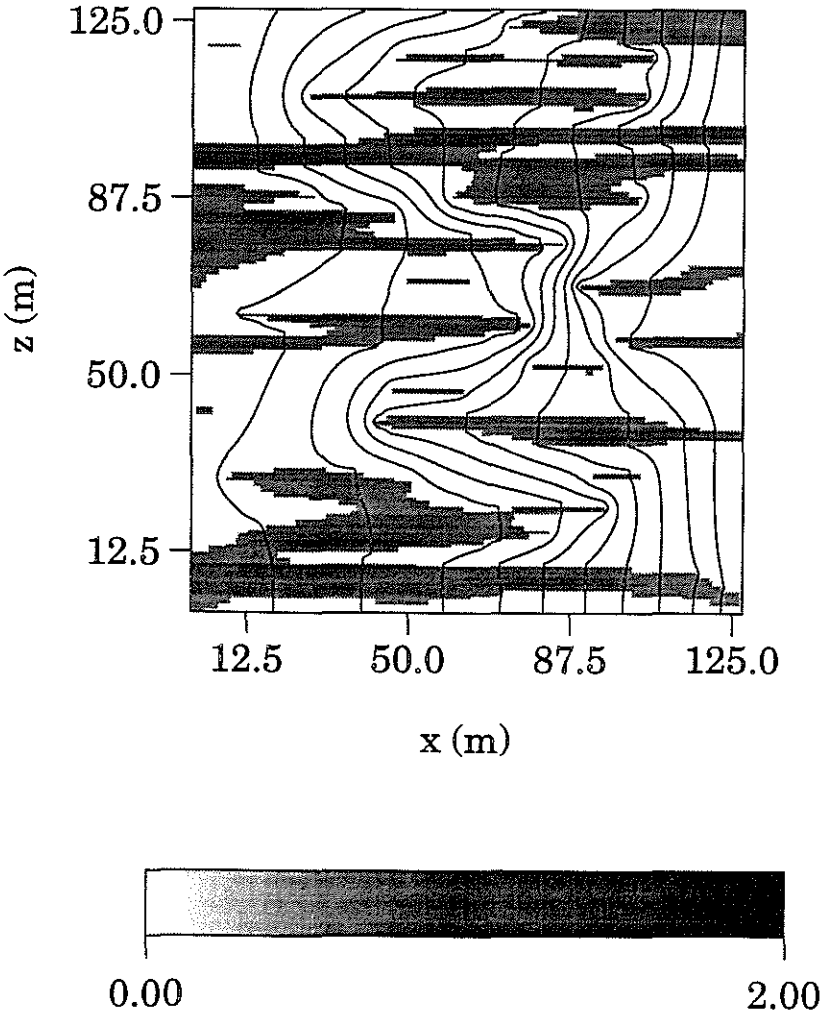

Figure 14: Random flow channel model and simulated pressure contours (solid curves).

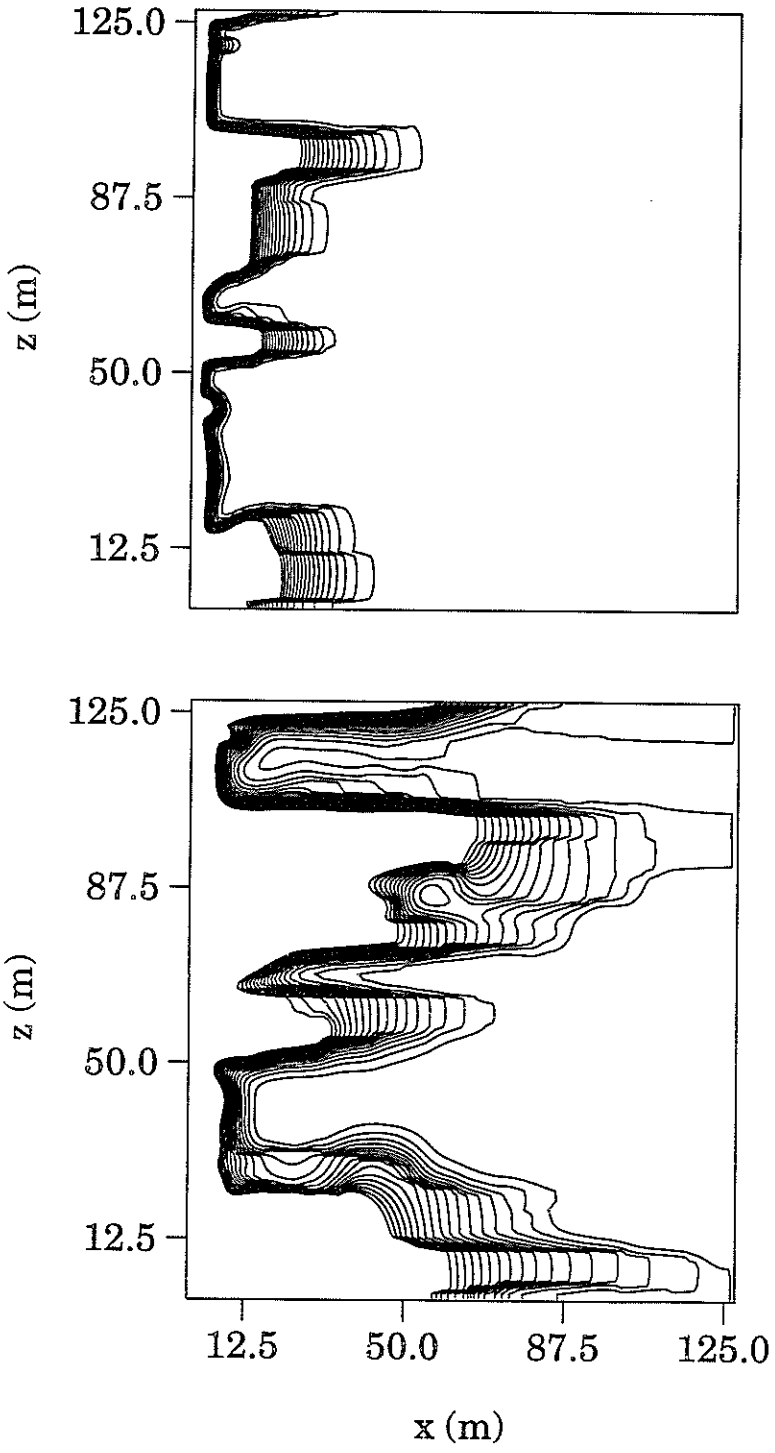

Figure 15: Solute concentration contours for the random flow channel model shown in Figure 14 and line pressure, line tracer sources. The upper figure is the concentration contour plot at $t \approx 14.12$ hours, the lower one is at $t \approx 2.94$ days.

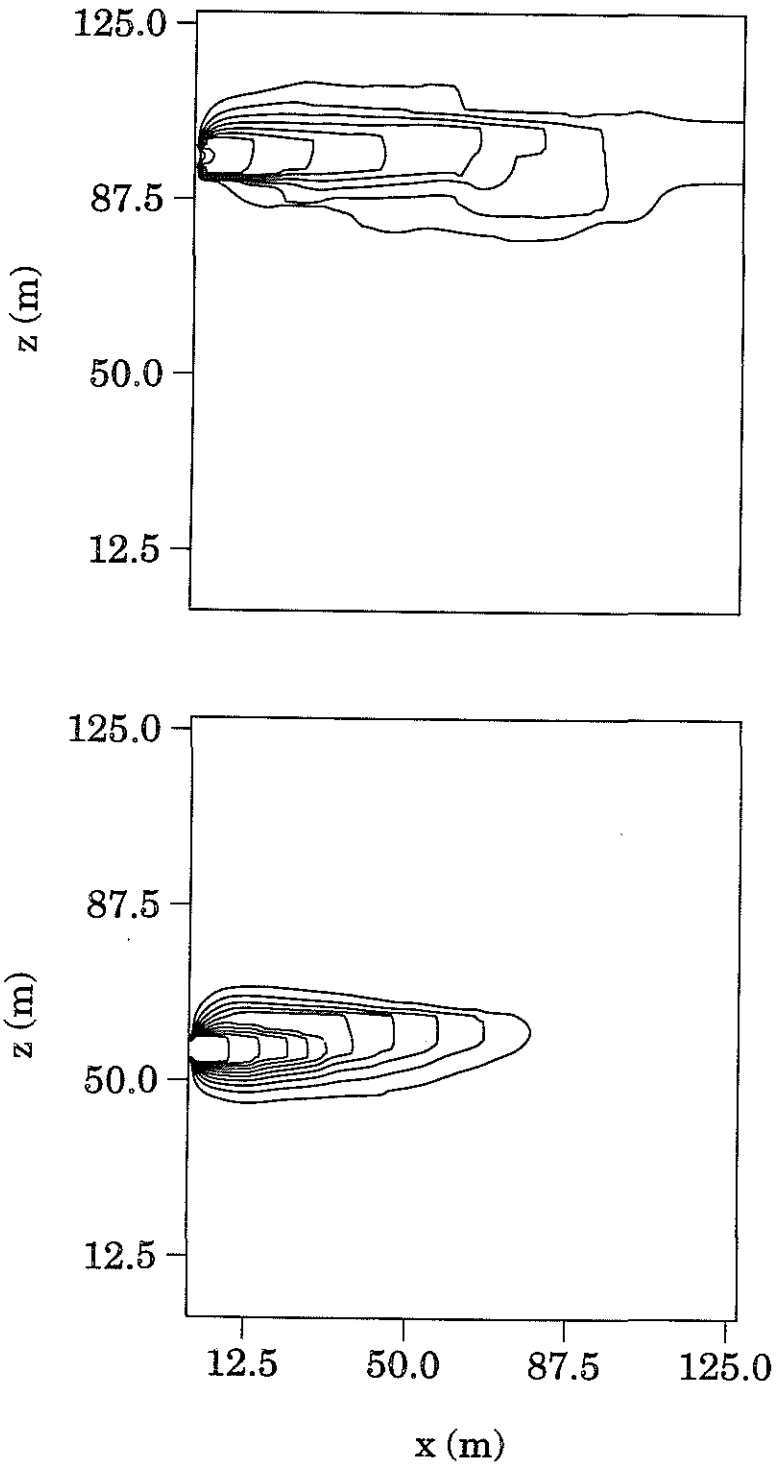

Figure 16: Solute concentration contours for the random flow channel model shown in Figure 14 and line pressure, point tracer sources. The tracer source is in a connected high permeability channel for the upper figure and in a terminated channel for the lower figure. The contours are plotted at $t \approx 5.88$ days in both figures.

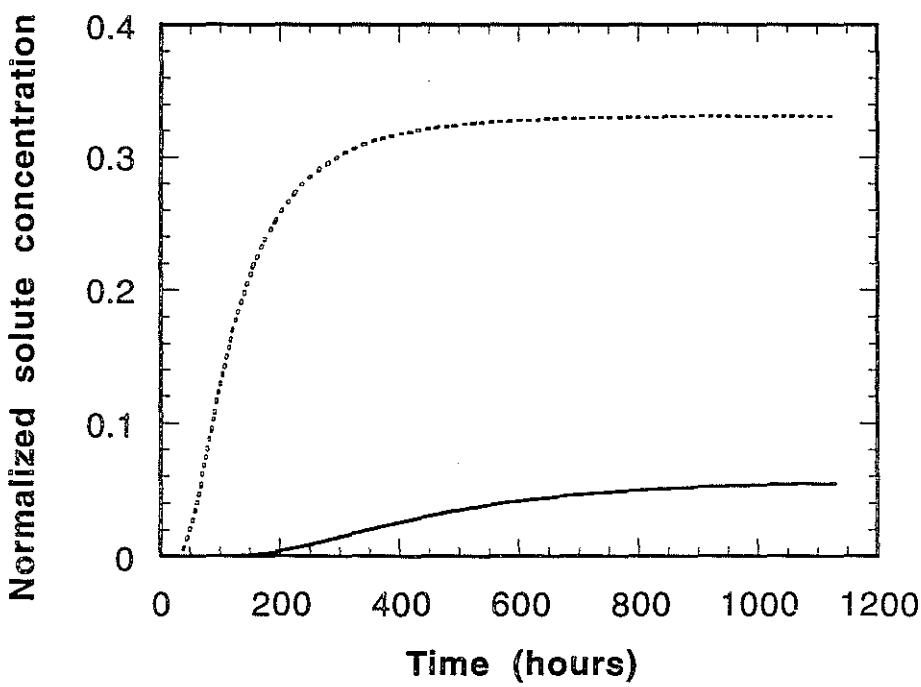

Figure 17: Solute mass received at two sites: one is in the connected channel (90, 98), the other is outside the channel (90, 57), for a point tracer source which is in a connected flow channel.

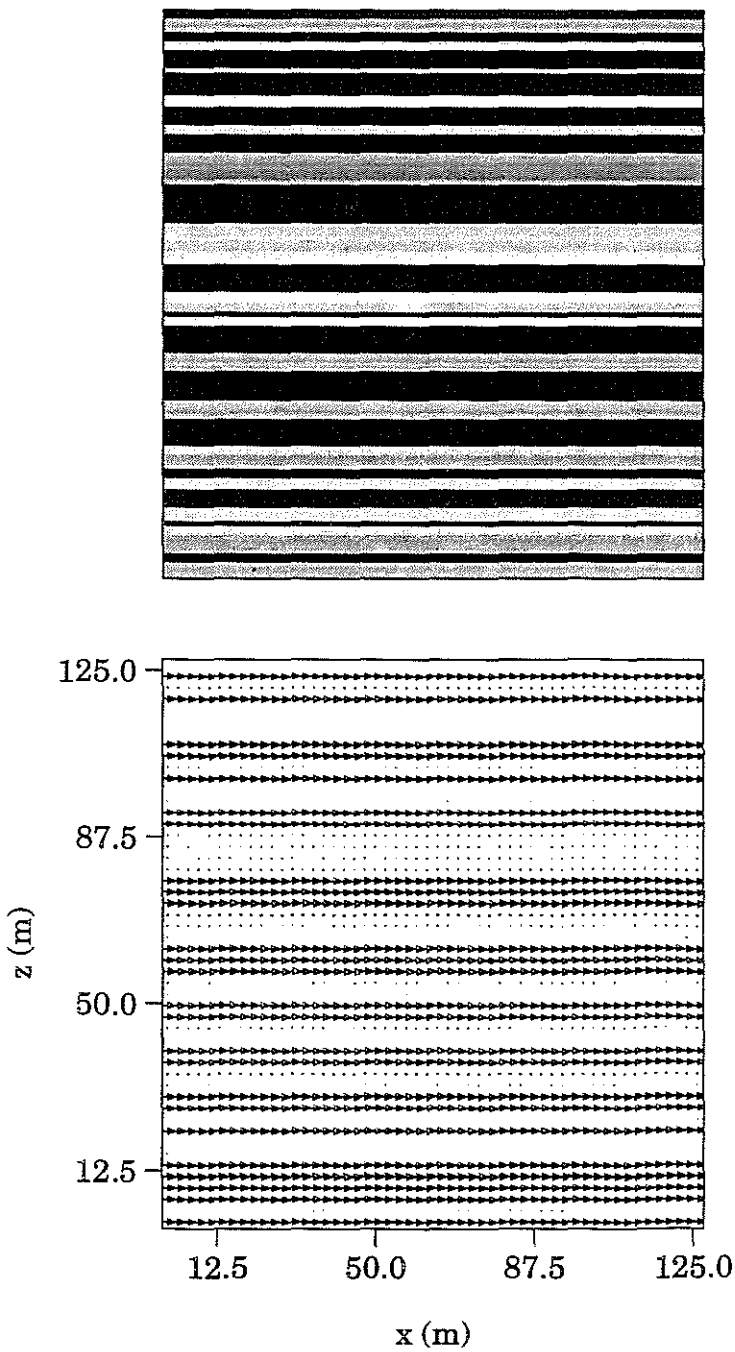

Figure 18: Poisson flow channel model (upper figure, the darker layers are the low permeability layers and the lighter layers are the high permeability layers) and simulated fluid flow field (lower figure).

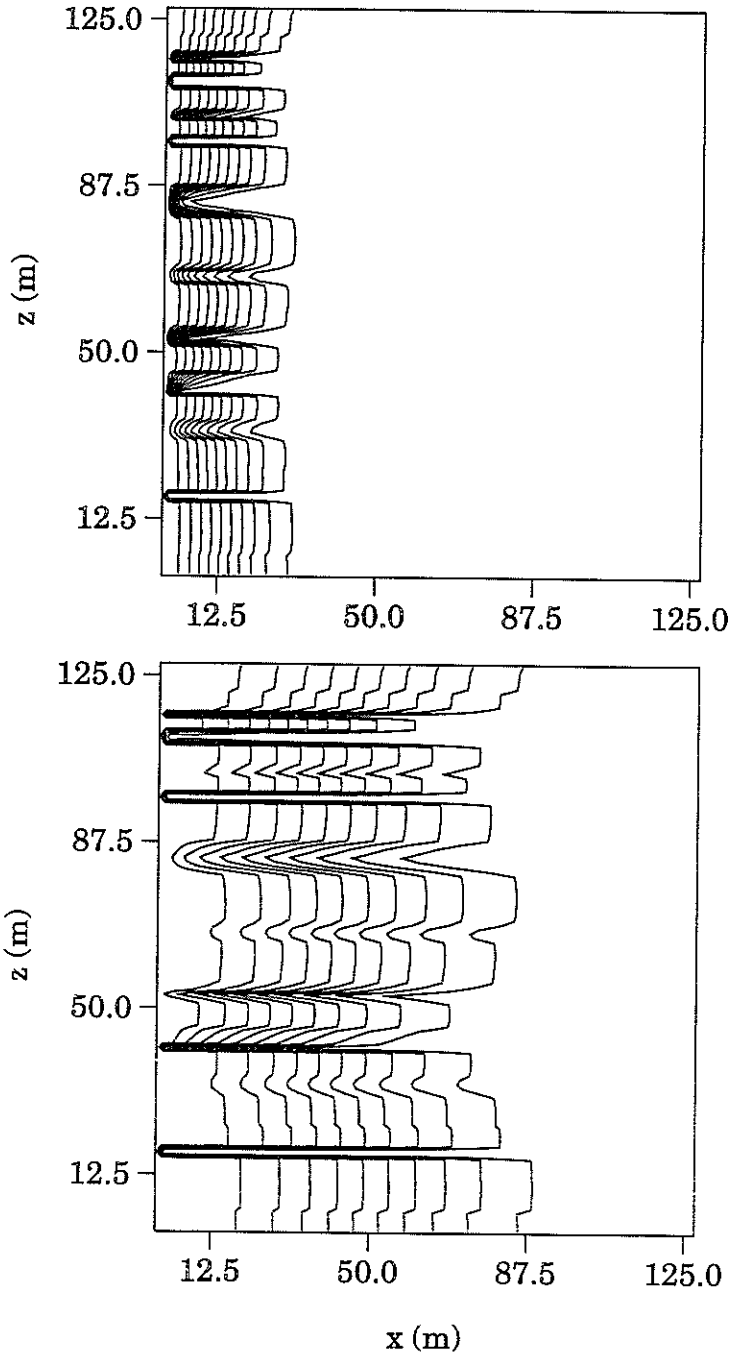

Figure 19: Solute concentration contours for the Poisson flow channel model shown in Figure 18 and line pressure and tracer sources. The upper figure is the concentration contour at $t \approx 14.12$ hours, the lower one is at $t \approx 2.94$ days.

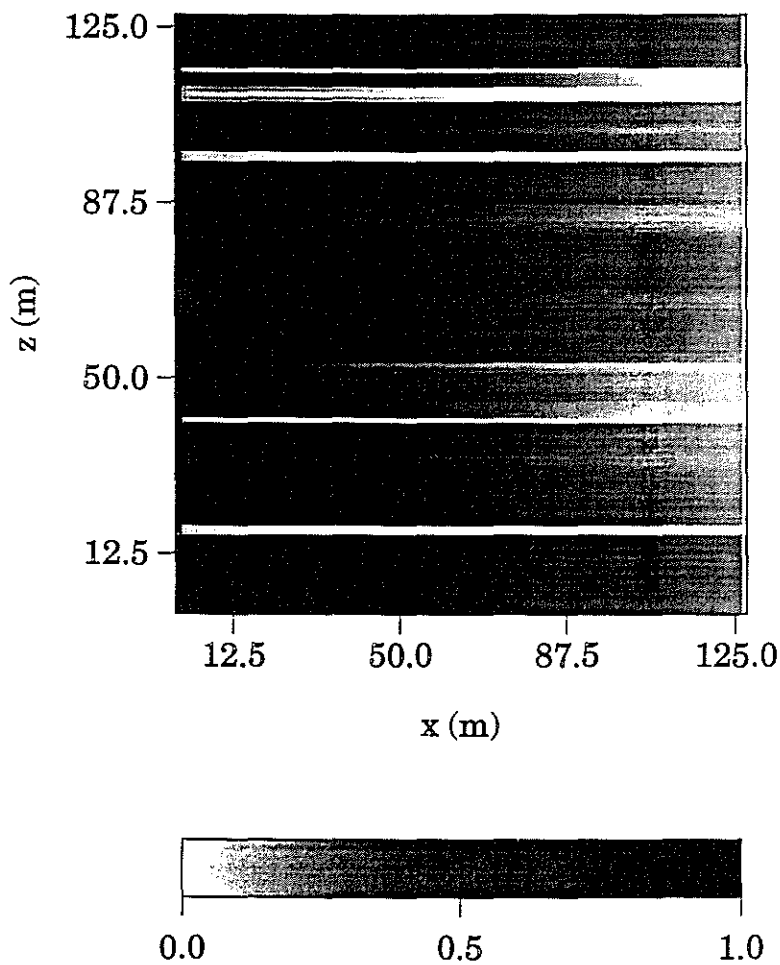

Figure 20: Solute concentration image for the Poisson flow channel model shown in Figure 18 and line pressure and tracer sources. at $t \approx 5.88$ days.

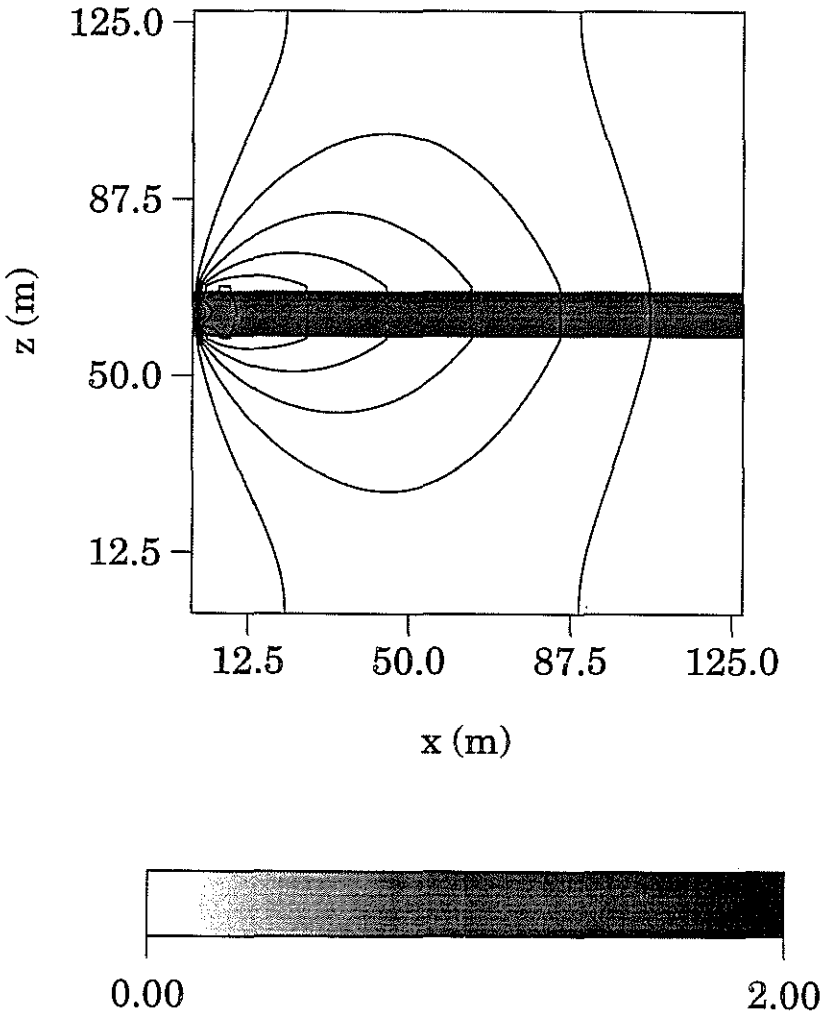

Figure 21: Single flow channel model and simulated pressure field (the contours). The channel width is 10 m and the model size is 127 × 127 m.

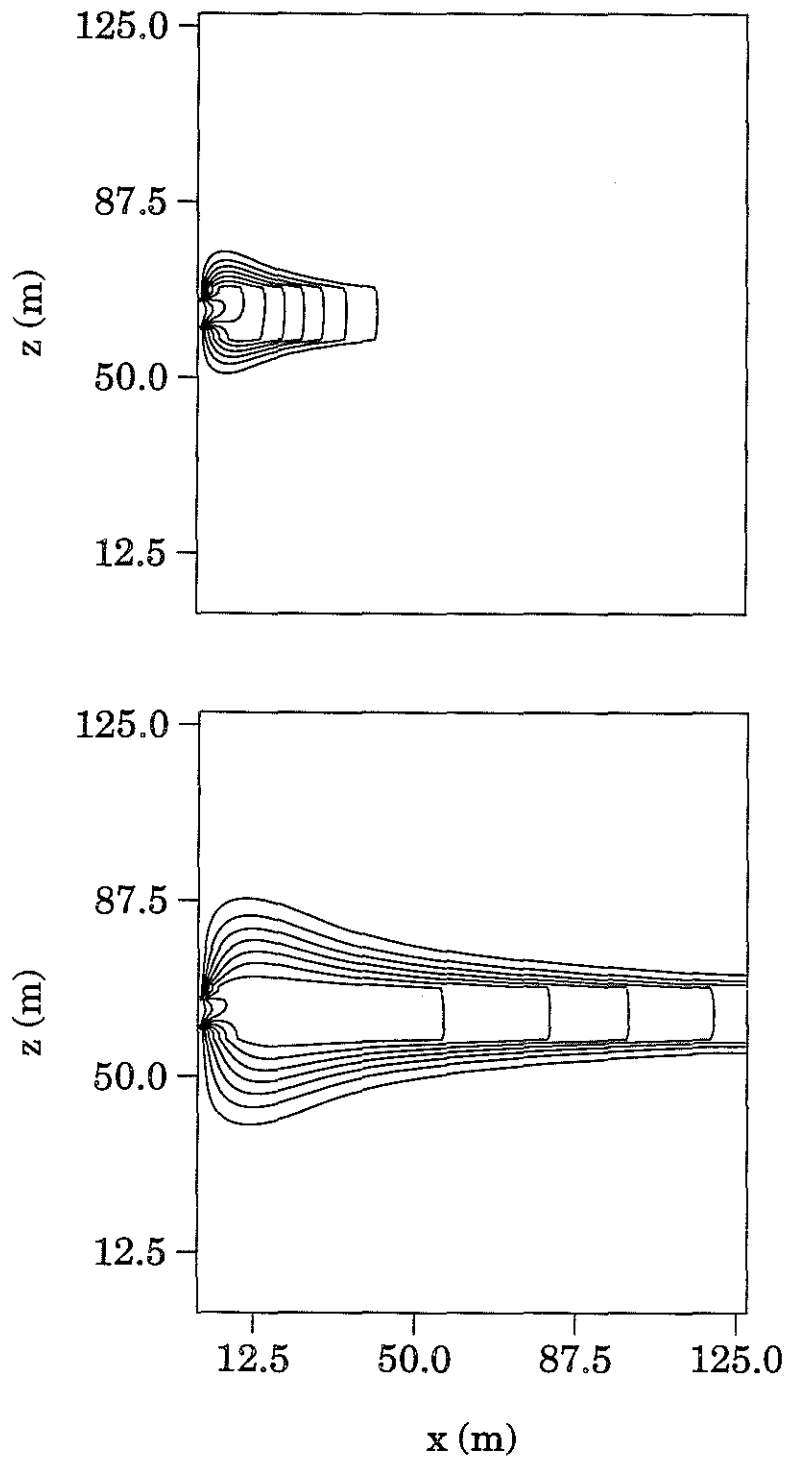

Figure 22: Solute concentration contours for the single flow channel model shown in Figure 21. The upper figure is the concentration contour at $t \approx 14.12$ hours, the lower one is at $t \approx 5.88$ days.

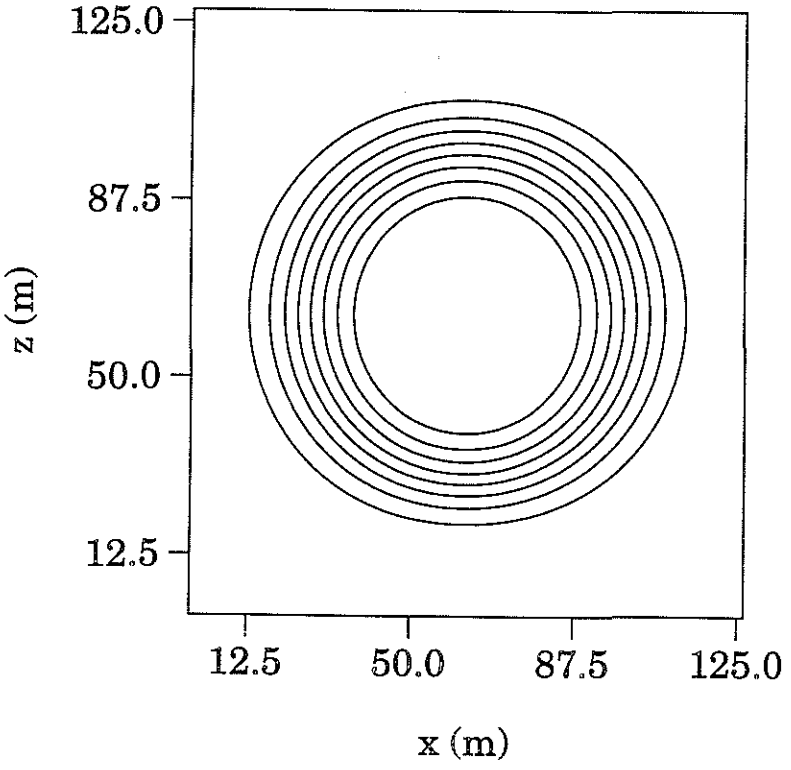

Figure 23: Concentration contours in a homogeneous medium for a point pressure and point tracer source at 8.82 days with symmetric boundary conditions.

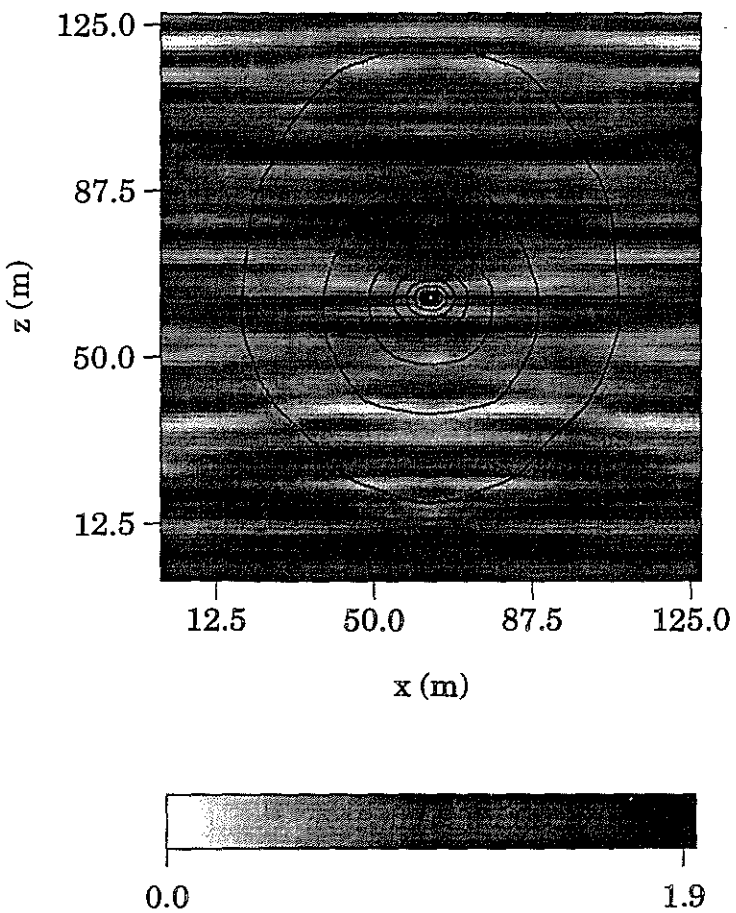

Figure 24: Aligned Gaussian model with a point pressure source in the middle together with the simulated pressure contours.

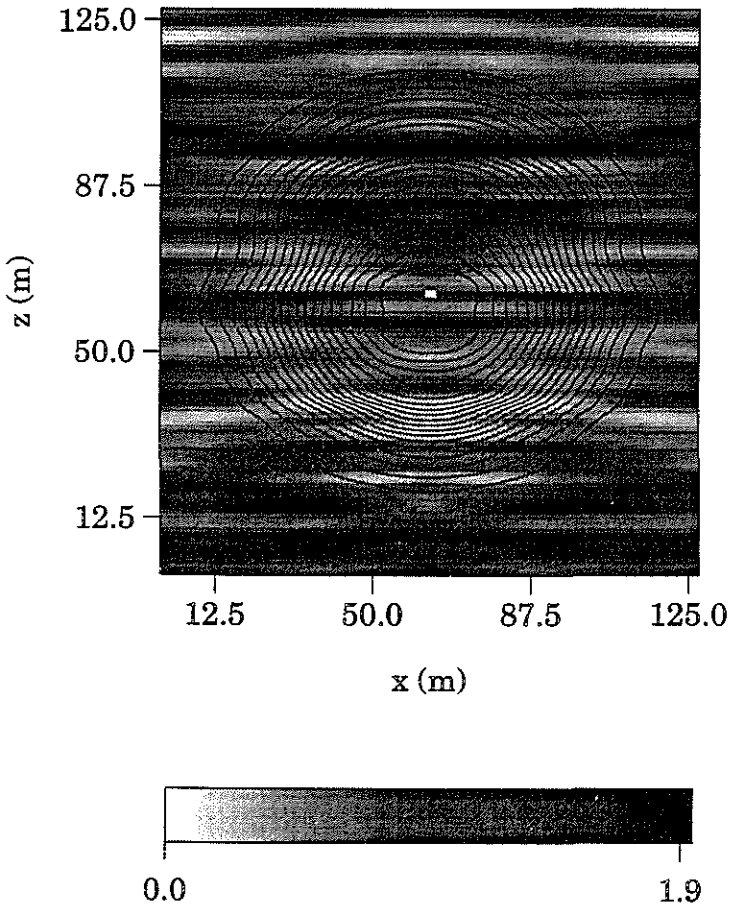

Figure 25: Solute concentration contours at t = 5.88 days for the model shown in Figure 24.

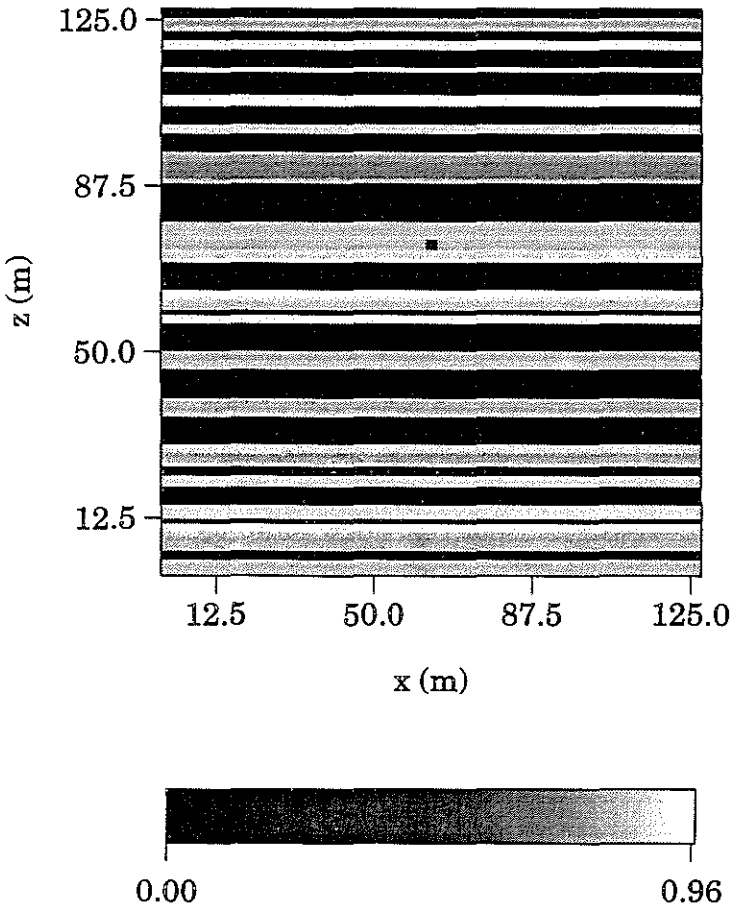

Figure 26: 1-D Poisson model with a point pressure source in a high permeable layer. The contours are the simulated pressure field.

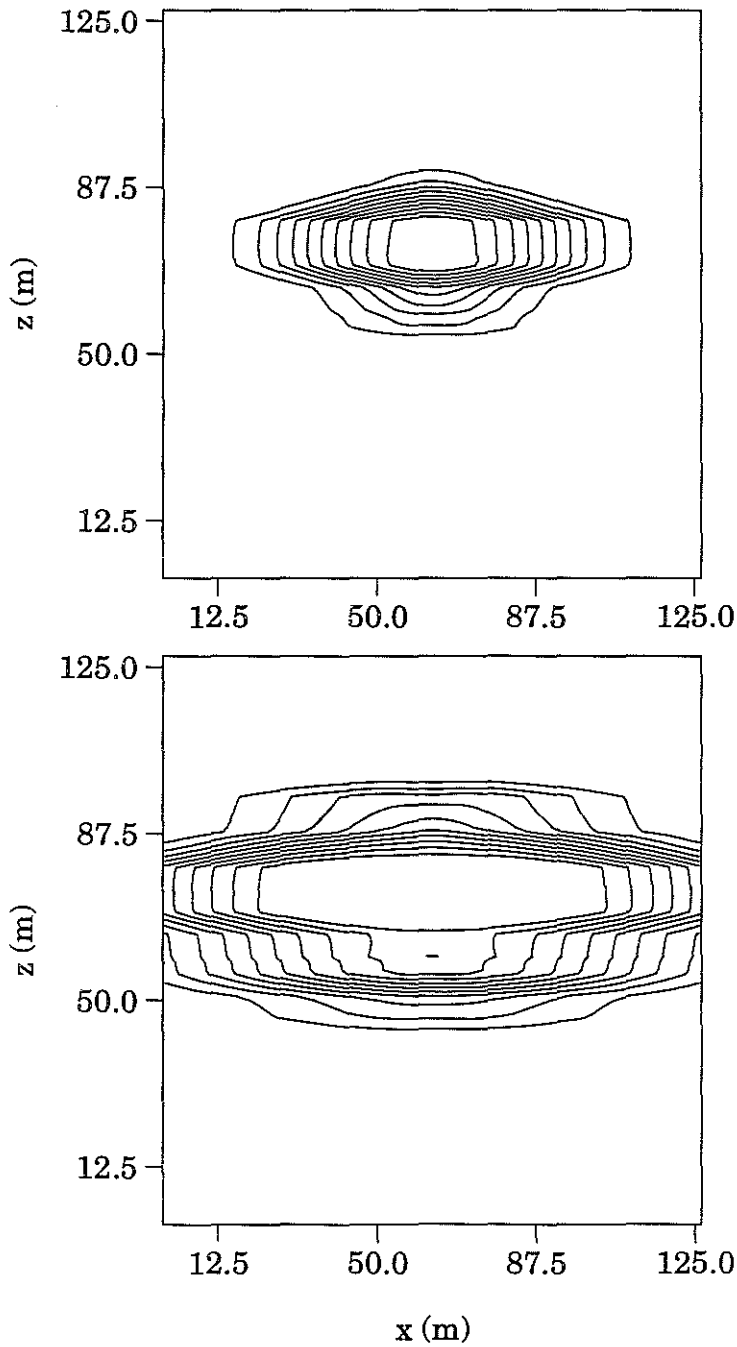

Figure 27: Solute concentration contours at t = 2.94 days and 11.76 days for the 1-D Poisson model shown in Figure 26 and point tracer source.

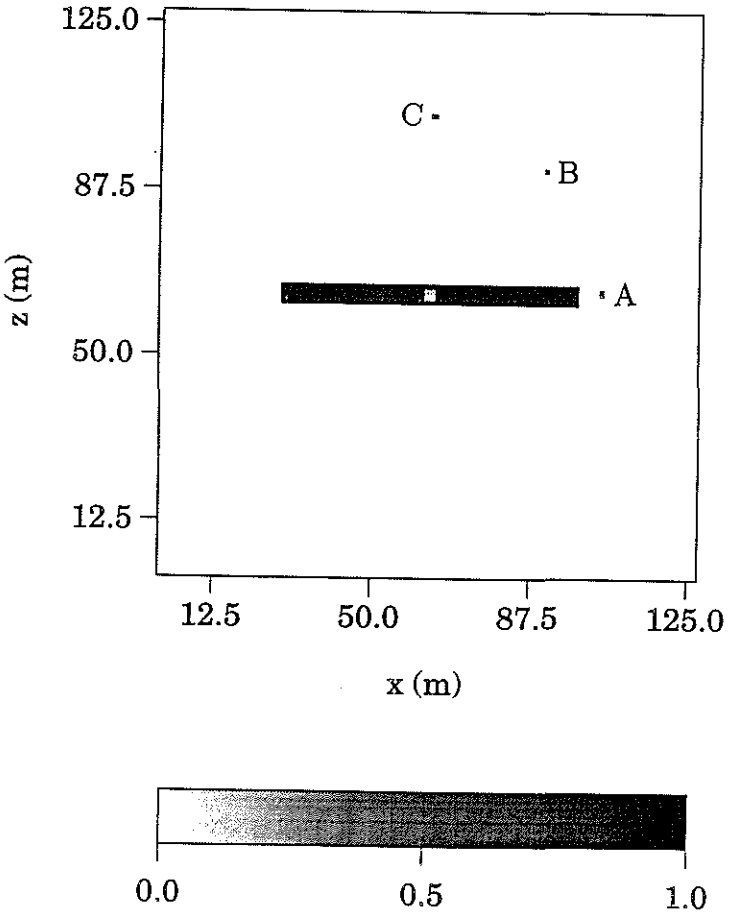

Figure 28: Single fracture model and the simulated pressure field (the contours). The three dots shown in the plot (A, B, and C) are the locations where we will receive the solute mass after a point tracer source is set up.

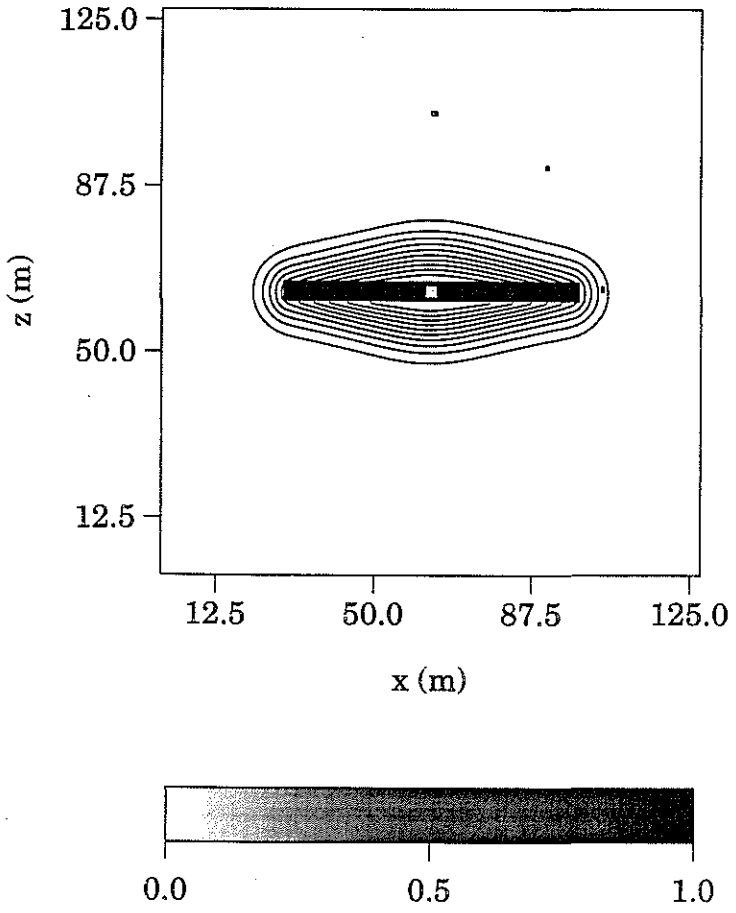

Figure 29: Solute concentration contours at t = 1.18 days for the model shown in Figure 28.

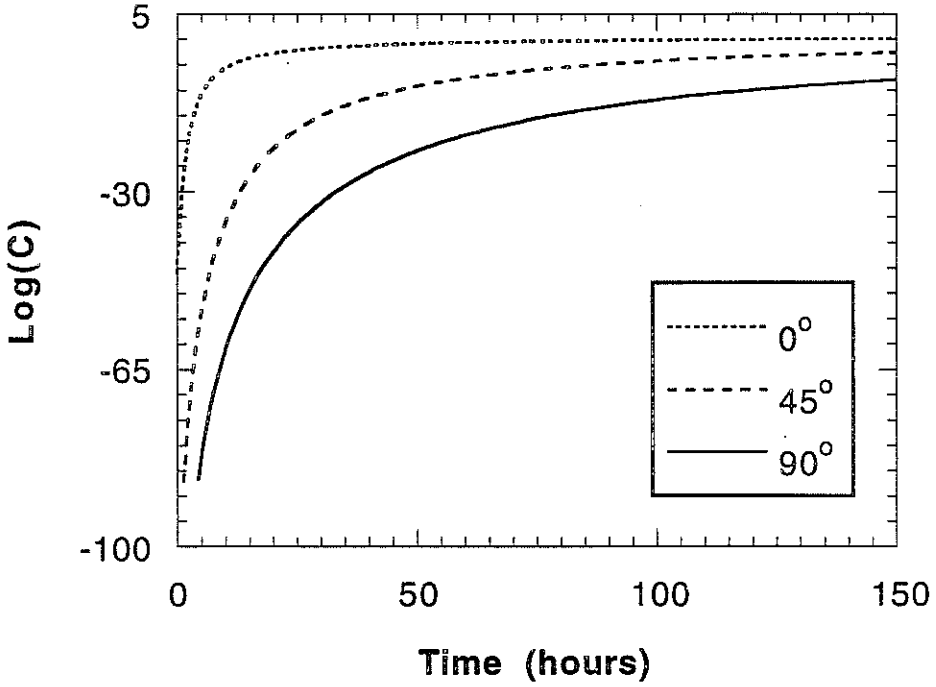

Figure 30: Solute mass received at points A (0°), B (45°), and C (90°) in Figure 29. The plot is in a semi-logarithm scale. We can see that the solute mass difference received at 0^o and 90^o is of the order of 10^4 at 150 hours.